Cell

Resurrection of endogenous retroviruses during aging reinforces senescence

Graphical abstract

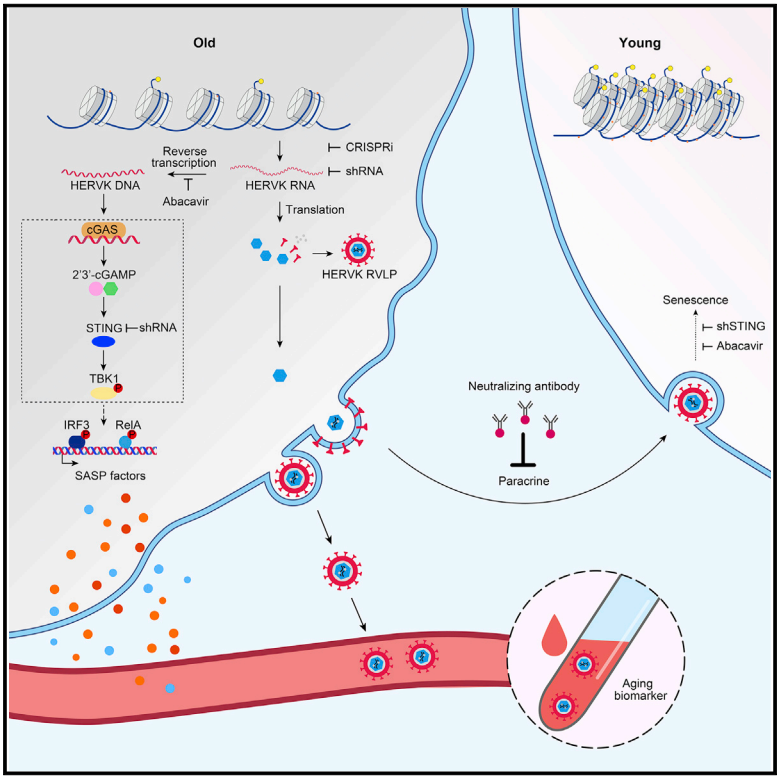

Highlights

- Derepression of the endogenous retrovirus contributes to programmed aging
- Upregulation of HERVK triggers the innate immune response and cellular senescence
- Extracellular HERVK retrovirus-like particles induce senescence in young cells
- Endogenous retrovirus serves as a potential target to alleviate aging

Authors

Xiaoqian Liu, Zunpeng Liu, Zeming Wu, ..., Weiqi Zhang, Jing Qu, Guang-Hui Liu

Correspondence

zhangwq@big.ac.cn (W.Z.), qujing@ioz.ac.cn (J.Q.), ghliu@ioz.ac.cn (G.-H.L.)

In brief

Liu and colleagues uncover the ways in which derepression of human endogenous retrovirus triggers cellular senescence and tissue aging; the findings provide fresh insights into therapeutic strategies for alleviating aging.

Liu et al., 2023, Cell *186*, 1–18
January 19, 2023
https://doi.org/10.1016/j.cell.2022.12.017

CellPress

Cell

CellPress

Article

Resurrection of endogenous retroviruses during aging reinforces senescence

Xiaoqian Liu,[1,5,6,7,21] Zunpeng Liu,[1,5,7,21] Zeming Wu,[2,5,7,21] Jie Ren,[3,5,7,21] Yanling Fan,[3,7] Liang Sun,[9] Gang Cao,[8] Yuyu Niu,[11,12,13] Baohu Zhang,[1,7] Qianzhao Ji,[2,7] Xiaoyu Jiang,[2,7] Cui Wang,[3,7] Qiaoran Wang,[3,7] Zhejun Ji,[1,5,7] Lanzhu Li,[2,7] Concepcion Rodriguez Esteban,[18] Kaowen Yan,[2,5,7] Wei Li,[4] Yusheng Cai,[2,5,7] Si Wang,[4,5,7,15,16] Aihua Zheng,[7,19] Yong E. Zhang,[7,14] Shengjun Tan,[14] Yingao Cai,[7,14] Moshi Song,[2,5,6,7] Falong Lu,[7,10] Fuchou Tang,[17] Weizhi Ji,[11,12,20] Qi Zhou,[1,5,6,7,20] Juan Carlos Izpisua Belmonte,[18,20] Weiqi Zhang,[3,5,7,*] Jing Qu,[1,5,6,7,*] and Guang-Hui Liu[2,4,5,6,7,22,*]

[1]State Key Laboratory of Stem Cell and Reproductive Biology, Institute of Zoology, Chinese Academy of Sciences, Beijing 100101, China
[2]State Key Laboratory of Membrane Biology, Institute of Zoology, Chinese Academy of Sciences, Beijing 100101, China
[3]CAS Key Laboratory of Genomic and Precision Medicine, Beijing Institute of Genomics, Chinese Academy of Sciences and China National Center for Bioinformation, Beijing 100101, China
[4]Advanced Innovation Center for Human Brain Protection, National Clinical Research Center for Geriatric Disorders, Xuanwu Hospital Capital Medical University, Beijing 100053, China
[5]Institute for Stem cell and Regeneration, Chinese Academy of Sciences, Beijing 100101, China
[6]Beijing Institute for Stem Cell and Regenerative Medicine, Beijing 100101, China
[7]University of Chinese Academy of Sciences, Beijing 100049, China
[8]State Key Laboratory of Agricultural Microbiology, Huazhong Agricultural University, Wuhan 430070, China
[9]NHC Beijing Institute of Geriatrics, NHC Key Laboratory of Geriatrics, Institute of Geriatric Medicine of Chinese Academy of Medical Sciences, National Center of Gerontology/Beijing Hospital, Beijing 100730, China
[10]State Key Laboratory of Molecular Developmental Biology, Institute of Genetics and Developmental Biology, The Innovative Academy of Seed Design, Chinese Academy of Sciences, Beijing 100101, China
[11]State Key Laboratory of Primate Biomedical Research, Institute of Primate Translational Medicine, Kunming University of Science and Technology, Kunming, Yunnan 650500, China
[12]Yunnan Key Laboratory of Primate Biomedical Research, Kunming, Yunnan 650500, China
[13]Faculty of Life Science and Technology, Kunming University of Science and Technology, Kunming, Yunnan 650500, China
[14]Key Laboratory of Zoological Systematics and Evolution, Institute of Zoology, Chinese Academy of Sciences, Beijing 100101, China
[15]Aging Translational Medicine Center, International Center for Aging and Cancer, Xuanwu Hospital, Capital Medical University, Beijing Municipal Geriatric Medical Research Center, Beijing 100053, China
[16]The Fifth People's Hospital of Chongqing, Chongqing 400062, China
[17]Peking-Tsinghua Center for Life Sciences, Peking University, Beijing 100871, China
[18]Altos Labs, Inc., San Diego, CA 94022, USA
[19]State Key Laboratory of Integrated Management of Pest Insects and Rodents, Institute of Zoology, Chinese Academy of Sciences, Beijing 100101, China
[20]Senior author
[21]These authors contributed equally
[22]Lead contact
*Correspondence: zhangwq@big.ac.cn (W.Z.), qujing@ioz.ac.cn (J.Q.), ghliu@ioz.ac.cn (G.-H.L.)
https://doi.org/10.1016/j.cell.2022.12.017

SUMMARY

Whether and how certain transposable elements with viral origins, such as endogenous retroviruses (ERVs) dormant in our genomes, can become awakened and contribute to the aging process is largely unknown. In human senescent cells, we found that HERVK (HML-2), the most recently integrated human ERVs, are unlocked to transcribe viral genes and produce retrovirus-like particles (RVLPs). These HERVK RVLPs constitute a transmissible message to elicit senescence phenotypes in young cells, which can be blocked by neutralizing antibodies. The activation of ERVs was also observed in organs of aged primates and mice as well as in human tissues and serum from the elderly. Their repression alleviates cellular senescence and tissue degeneration and, to some extent, organismal aging. These findings indicate that the resurrection of ERVs is a hallmark and driving force of cellular senescence and tissue aging.

Please cite this article in press as: Liu et al., Resurrection of endogenous retroviruses during aging reinforces senescence, Cell (2023), https://doi.org/10.1016/j.cell.2022.12.017

INTRODUCTION

Aging is associated with a physiological decline and manifestations of chronic diseases, yet many of its underlying molecular changes and mechanisms remain poorly understood. With significant efforts over the past decades, several causal determinants of aging-related molecular changes have been identified, such as epigenetic alterations and stimulation of senescence-associated secretory phenotype (SASP) factors.[1–7] Although the majority of these studies describe aging determinants originating primarily from protein-coding genes, the non-coding part of the genome has started to garner attention as well. For example, silent long-interspersed element-1 (LINE1) retrotransposons, belonging to non-long terminal repeat (non-LTR) retrotransposons, can be activated during senescence, triggering the innate immune response that is responsible for part of the senescence-associated phenotypes.[8–15]

A different class of retroelements, endogenous retroviruses (ERVs), belonging to LTR retrotransposons are a relic of ancient retroviral infection, fixed in the genome during evolution, comprising about 8% of the human genome.[16–19] As a result of evolutionary pressure, most human ERVs (HERVs) accumulate mutations and deletions that prevent their replication and transposition function.[20,21] However, some evolutionarily young subfamilies of HERV proviruses, such as the recently integrated HERVK human mouse mammary tumor virus like-2 (HML-2) subgroup, maintain open reading frames encoding proteins required for viral particle formation, including Gag, Pol, Env, and Pro.[18,22] Except at specific stages of embryogenesis when DNA is hypomethylated and under certain pathological conditions such as cancer,[23–27] HERVs are transcriptionally silenced by host surveillance mechanisms such as epigenetic regulation in post-embryonic developmental stages. [28,29] Notably, whether ERVs can escape host surveillance during aging and, if so, what effects they may exert on cellular and organismal aging are still poorly investigated.

In this study, using cross-species models and multiple techniques, we revealed an uncharacterized role of endogenous retrovirus resurrection as a biomarker and driver for aging. Specifically, we identified endogenous retrovirus expression associated with cellular and tissue aging and that the accumulation of HERVK retrovirus-like particles (RVLPs) mediates the aging-promoting effects in recipient cells. More importantly, we can inhibit endogenous retrovirus-mediated pro-senescence effects to alleviate cellular senescence and tissue degeneration *in vivo*, suggesting possibilities for developing therapeutic strategies to treat aging-related disorders.

RESULTS

Upregulated HERVK expression in senescent hMPCs is associated with epigenetic derepression

Cellular senescence is considered a major contributing factor to aging and a hallmark of human progeroid diseases, i.e., Hutchinson-Gilford progeria syndrome (HGPS) and Werner syndrome (WS).[2,30–36] We previously demonstrated that HGPS human mesenchymal progenitor cells (hMPCs) (*LMNA*$^{G608G/+}$ hMPCs) or WS hMPCs (*WRN*$^{-/-}$ hMPCs) recapitulated premature aging phenotypes (Figure 1A), characterized by increased senescence-associated β-galactosidase (SA-β-gal)-positive cells (Figure S1A). Reduced cellular proliferation rates were also observed in HGPS and WS hMPCs, as well as in replicatively senescent (RS) wild-type (WT) hMPCs, as evidenced by fewer Ki67-positive cells and decreased clonal expansion ability (Figures S1B–S1F).[31–35,37]

Here, we leveraged these premature aging models to test whether the activation of the ERVs is associated with human cellular senescence. We found an increased expression of several transposable elements in senescent hMPCs, such as LTRs (Figures 1B and S1G; Table S1). Specifically, we found that retroelement HERVK internal coding sequences (HERVK-int) were upregulated in both replicatively and prematurely senescent hMPCs (Figures 1C and S1H; Table S1). Using primers targeting different regions of HERVK transcripts, including *env*, *pol*, and *gag*, we confirmed by quantitative reverse transcriptase PCR (qRT-PCR) that HERVK retroelements were highly expressed during cellular senescence, with a similar increase of the senescence marker p21^{Cip1} (*CDKN1A*), whereas lamina-associated protein LAP2 (*TMPO*) decreased during senescence as reported previously (Figure 1D).[38] Likewise, an RNA fluorescence *in situ* hybridization (RNA-FISH) analysis also showed increased HERVK RNA signals in HGPS and WS hMPCs (Figure S1I). When we performed single-molecule RNA-FISH (smRNA-FISH) with different fluorescent probes targeting *LTR5_Hs*, *env*, and *pol*, we detected co-staining signals in close proximity, implying that mRNA molecules harboring *LTR5_Hs* (the transcriptional regulatory region of HERVK), *env*, and *pol* are present in senescent hMPCs (Figure 1E).

Consistent with the increased expression of HERVK transcription in senescent hMPCs, we observed reduced CpG DNA methylation levels in HERVK-int regions and those HERVK proviral loci (Figures 1F, S1J, and S1K),[39,40] alongside a decrease in the repressive histone mark (H3K9me3) and an increase in the transcriptionally active histone mark (H3K36me3) at HERVK-*LTR5_Hs* (Figures 1G and S1L). These data indicate that the epigenetic derepression of HERVK, likely contributing to HERVK transcription, is associated with cellular senescence.

Accumulation of viral proteins and RVLPs of HERVK in various types of senescent human cells

Next, we asked whether elevated endogenous retrovirus expression would elicit the production of HERVK protein components and even the formation of RVLPs. Western blotting and immunofluorescence staining analyses showed increased HERVK-Env protein levels in both prematurely senescent and RS hMPCs (Figures 2A, 2B, and S2A). Moreover, by co-staining HERVK-Env with SPiDER-βGal or p21^{Cip1}, we found that the elevation of HERVK-Env was more pronounced in the senescent cell population (Figures S2B and S2C). In line with the increased levels of HERVK mRNA and protein, we detected an accumulation of RVLPs in the cytoplasm of both prematurely senescent and RS hMPCs by transmission electron microscopy (TEM) analysis; by contrast, RVLPs were very rare in early-passage WT hMPCs that were phenotypically young (Figures 2C and S2D). Using immuno-TEM analysis with an anti-HERVK-Env antibody,[41] we found that these RVLPs, with a diameter ranging from 80 to 120 nm, were labeled with HERVK-Env antibody in senescent cells (Figures 2D,

Please cite this article in press as: Liu et al., Resurrection of endogenous retroviruses during aging reinforces senescence, Cell (2023), https://doi.org/10.1016/j.cell.2022.12.017

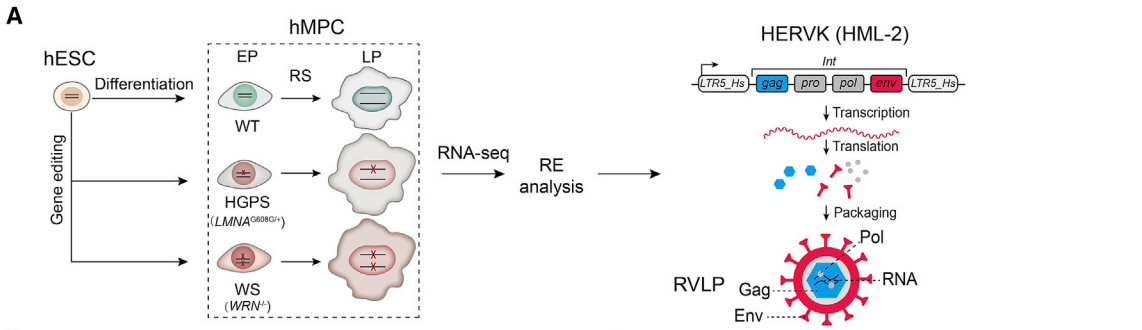

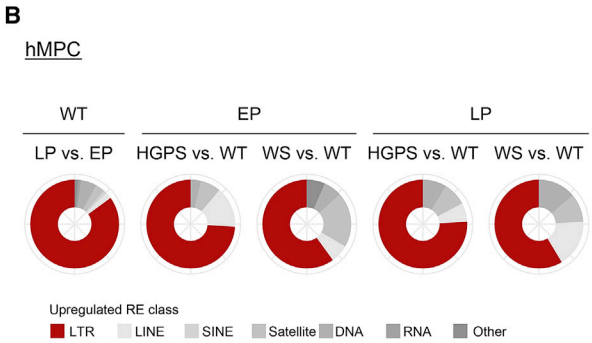

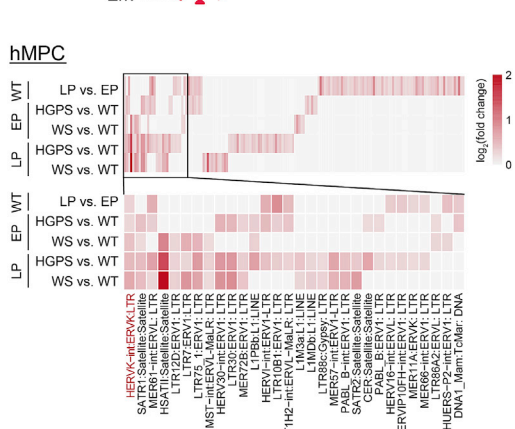

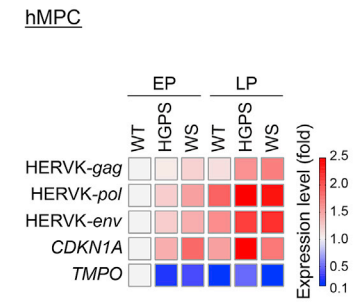

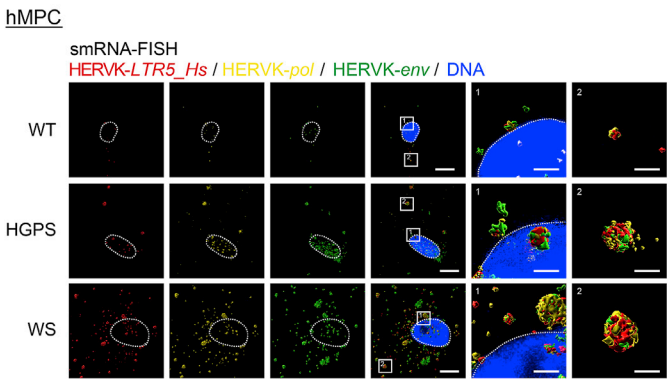

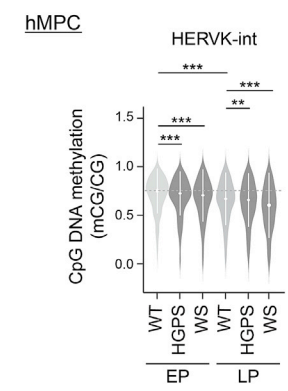

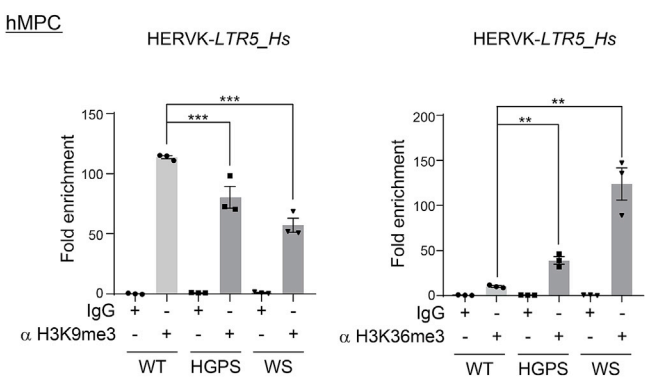

(legend on next page)

Please cite this article in press as: Liu et al., Resurrection of endogenous retroviruses during aging reinforces senescence, Cell (2023), https://doi.org/10.1016/j.cell.2022.12.017

S2E, and S2F). These findings demonstrate the increased production of both viral proteins and RVLPs of HERVK in senescent hMPCs.

In order to verify the expression of HERVK in other senescent cell types, we isolated primary human fibroblasts and hMPCs. Similar to senescent hMPC models, we observed increased HERVK-Env protein levels in the RS primary fibroblasts (Figures 2E, 2F and S2G–S2I). In addition, we found decreased occupancy of H3K9me3 and increased occupancy of H3K36me3 at HERVK-*LTR5_Hs* in human fibroblasts during replicative senescence (Figure 2G). We also observed an increased accumulation of RVLPs in these senescent primary fibroblasts (Figure 2H). Furthermore, we found prominent HERVK expression evidenced by a more than 5-fold increase in transcript levels in primary hMPCs derived from old individuals compared with their younger counterparts (Figures 2I and S2J; Table S2). Collectively, through multimodal experiments, we verified aberrant HERVK expression, as well as viral protein and RVLP accumulation in senescent cells.

Increased expression of HERVK drives cellular senescence

To determine how the activation of endogenous HERVK affects cellular senescence, we used a CRISPR-dCas9-mediated transcriptional activation (CRISPRa) system containing activation protein complexes (synergistic activation mediators [SAMs]) with sgRNAs targeting the HERVK-*LTR5_Hs* promoter regions in WT hMPCs (Figure S3A).[42] We confirmed the activation of HERVK endogenous retrotransposon elements by qRT-PCR and western blotting (Figures 3A and S3B). We found that targeted HERVK activation induced hMPC senescence, as evidenced by the induction of classic senescent features (Figures 3B, 3C, S3B, and S3C). To further assess whether suppression of endogenous HERVK inhibited cellular senescence, we used the CRISPR-dCas9-KRAB transcriptional inactivation (CRISPRi) system[43] (Figures 3D, S3D, and S3E) to repress HERVK in prematurely senescent hMPCs and found that targeted HERVK repression alleviated hMPC senescence (Figures 3E, 3F, S3E, and S3F). In addition, the knockdown of HERVK using HERVK-interfering shRNA[44,45] also antagonized premature senescence (Figures 3G, 3H, and S3G–S3I).

Given the observed aging-associated decrease of DNA methylation at the HERVK loci in hMPCs (Figures 1F and S1K), we conducted an independent experiment in which we treated early-passage WT hMPCs with the DNA methyltransferase inhibitor (DNMTi) 5-azacytidine (5-AZA) to mimic aging-related global hypomethylation (Figure 3I).[46,47] A whole-genome bisulfite sequencing (WGBS) analysis confirmed reduced CpG DNA methylation levels at HERVK elements after treatment (Figures 3J and S3J). Consistent with targeted HERVK activation by the CRISPRa system, 5-AZA treatment also led to upregulated HERVK RNA levels concomitant with premature cellular senescence phenotypes (Figures 3K–3M and S3K). By contrast, these senescence phenotypes were abrogated by HERVK knockdown (Figures S3L–S3N), suggesting that 5-AZA triggers cellular senescence at least partially via the DNA demethylation-induced transcriptional activation of HERVK. Moreover, we also activated endogenous HERVK in primary hMPCs derived from a young individual via CRISPRa or 5-AZA treatment (Figures S3O and S3P) and found that transcriptional activation of HERVK accelerated cellular senescence (Figures 3N–3Q). Taken together, through the disruption of the host epigenetic mechanism and targeted manipulation of HERVK transcriptional activity, we revealed that enhanced levels of endogenous HERVK are a driver of hMPC senescence.

HERVK expression triggers the innate immune response

HERVK-encoded Pol protein possesses reverse transcription activity that can reverse-transcribe HERVK RNA into DNA,[16,17] thereby generating additional HERVK DNA outside of the genome. Consistent with increased HERVK RNA (Figures 1D and S1I), we also observed increased HERVK DNA in the cytoplasm of senescent hMPCs by single-molecule DNA-FISH (Figures 4A and S4A). Therefore, we suspected that such excessive cytoplasmic DNA might be recognized by the DNA sensor cGMP-AMP synthase (cGAS) and trigger activation of the innate immune system (Figure 4B).[48–50] Indeed, by immunoprecipitation analysis, we verified the marked enrichment of cGAS on cytoplasmic HERVK DNA in senescent hMPCs, which was not the case in early-passage young hMPCs (Figure 4C). Supporting cytosolic HERVK DNA triggering the activation of the cGAS-Stimulator of interferon genes (STING) pathway, we detected increases in 2′3′-cGAMP content (Figure 4D) and the phosphorylation of TANK-binding kinase 1 (TBK1), RelA, and IFN regulatory factor 3 (IRF3) (Figure 4E). We also observed the upregulation of inflammatory cytokines, including *IL1B* (IL1β) and *IL6*, both of which are classified as SASP factors[51,52] (Figures 4F, 4G, and S4B; Table S3) in prematurely senescent hMPCs. The activation of the cGAS-STING-mediated innate immune response was also revealed in RS hMPCs (Figures S4C–S4E; Table S3) and RS fibroblasts (Figures S4F–S4H).

Consistently, the inhibition of HERVK via shRNA decreased the phosphorylation levels of TBK1 and RelA (Figure 4H). In addition, blocking one downstream effector of HERVK activation via the knockdown of STING reduced both the inflammatory response and SASP expression (Figures 4I and S4I), thus

Figure 1. Epigenetic derepression of HERVK is observed in senescent hMPCs

(A) Schematic diagram of human stem cell aging models and the HERVK proviral genome structure.

(B and C) Ring plots showing the percentages of upregulated repetitive elements in each class (B) and heatmap showing the relative expression levels for upregulated RepeatMasker-annotated repetitive elements (C) in RS and prematurely senescent hMPCs at early passage (EP) and late passage (LP).

(D) Heatmap showing the levels of HERVK transcripts and senescence marker genes in WT, HGPS, and WS hMPCs at EP and LP as detected by qRT-PCR.

(E) Representative z stack three-dimensional (3D) reconstruction images of smRNA-FISH in WT, HGPS, and WS hMPCs with probes targeting HERVK-*LTR5_Hs*, -*pol*, and -*env* with different fluorophores.

(F) Violin plot showing the CpG DNA methylation levels for HERVK-int in RS and prematurely senescent hMPCs.

(G) ChIP-qPCR analysis of H3K9me3 and H3K36me3 enrichment in HERVK-*LTR5_Hs* regions in WT, HGPS, and WS hMPCs.

Scale bars, 10 μm and 100 nm (zoomed-in image) in (E).

See also Figure S1 and Table S1.

Please cite this article in press as: Liu et al., Resurrection of endogenous retroviruses during aging reinforces senescence, Cell (2023), https://doi.org/10.1016/j.cell.2022.12.017

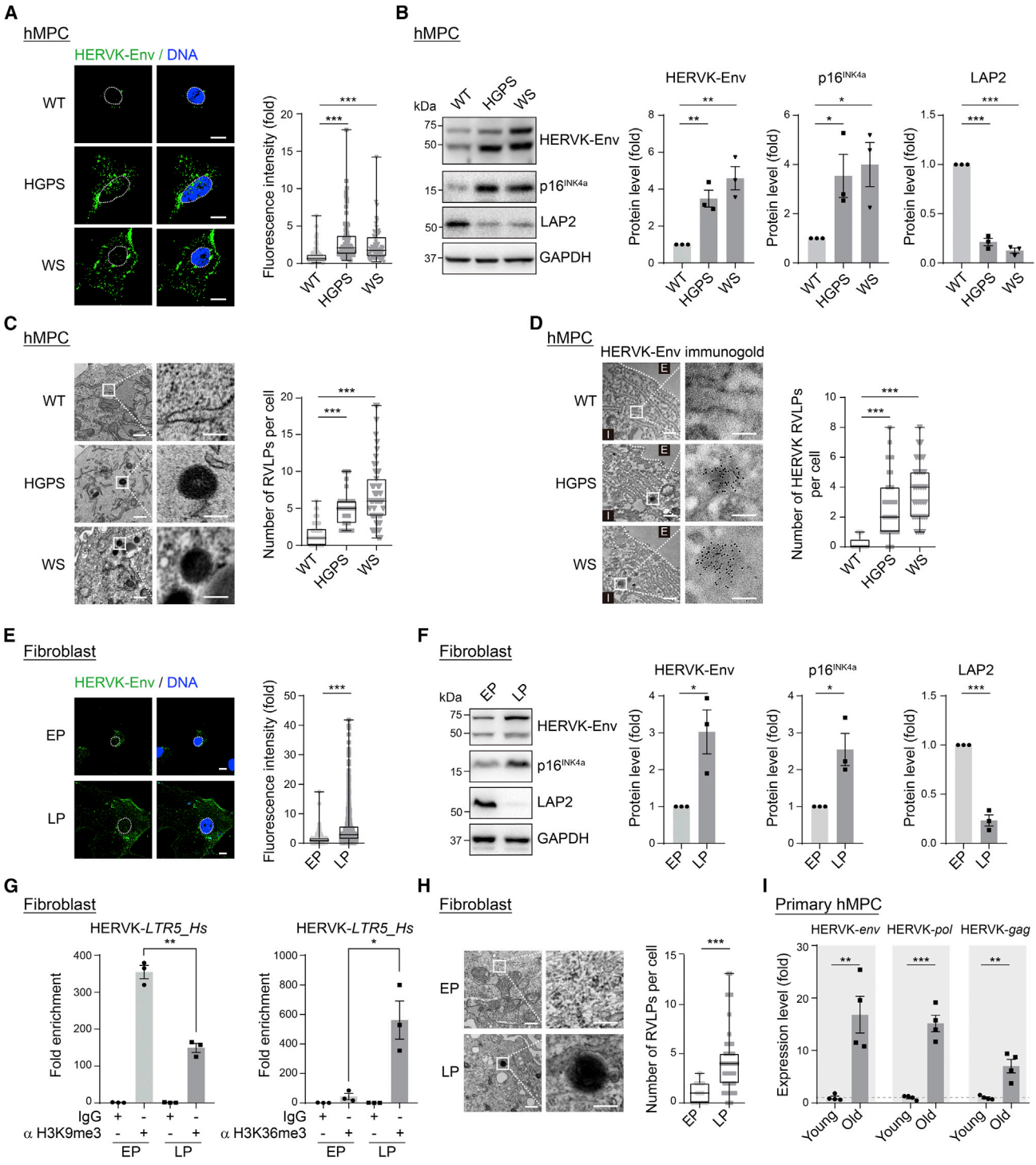

Figure 2. HERVK viral proteins and RVLPs are increased in senescent cells

(A) Immunofluorescence staining of HERVK-Env in WT, HGPS, and WS hMPCs.

(B) Western blotting of HERVK-Env, p16^{INK4a}, and LAP2 in WT, HGPS, and WS hMPCs.

(C) TEM analysis of WT, HGPS, and WS hMPCs.

(D) TEM analysis after immunogold labeling with anti-HERVK-Env antibody in WT, HGPS, and WS hMPCs. E, Extracellular; I, Intracellular.

(E) Immunofluorescence staining of HERVK-Env in primary human fibroblasts at EP and LP.

(F) Western blotting of HERVK-Env, p16^{INK4a}, and LAP2 in primary human fibroblasts at EP and LP.

(G) ChIP-qPCR analysis of H3K9me3 and H3K36me3 enrichment in HERVK-*LTR5_Hs* regions in primary human fibroblasts at EP and LP.

(legend continued on next page)

Please cite this article in press as: Liu et al., Resurrection of endogenous retroviruses during aging reinforces senescence, Cell (2023), https://doi.org/10.1016/j.cell.2022.12.017

alleviating cellular senescence in prematurely senescent hMPCs (Figure 4J). Moreover, we also blocked the downstream effect through Abacavir, a potent nucleoside reverse transcriptase inhibitor that can inhibit the activity of HERVK-encoded Pol (Figure 4K).[53] Senescent hMPCs treated with Abacavir demonstrated diminished HERVK DNA content (Figure 4L), along with substantial alleviation of a panel of senescence-associated phenotypes (Figures 4M–4O, S4J, and S4K). In contrast to the loss-of-function experiments described above, the activation of endogenous HERVK via the CRISPRa system or 5-AZA treatment led to an augmented innate immune response and upregulated expression of SASP cytokines in young WT hMPCs (Figures 4P–4S, S4L, and S4M; Table S4). These findings place the increased expression of HERVK as a contributing factor for cellular senescence, at least in part by triggering innate immune responses.

Extracellular HERVK RVLPs induce cellular senescence

Previous studies indicated that tumor cell-derived HERVK RVLPs could be released into the culture medium and then taken up by other cells.[54] Given that the presence of HERVK RVLPs in senescent cells was observed in this study (Figures 2C, 2D, and S2D–S2F), we asked whether HERVK RVLPs produced by senescent cells could be released extracellularly and convey senescence signals to non-senescent cells (Figure 5A). To answer this question, we employed the sensitive droplet digital PCR (ddPCR) technology[55] to detect HERVK RNA (the genetic material that is supposed to be packaged in RVLPs) in conditioned medium (CM) harvested from WT and prematurely senescent hMPCs. In CM from prematurely senescent hMPCs, we found that the HERVK RNA level was 5 to 12 times higher than that in CM from young WT hMPCs (Figure 5B). In addition, both enzyme-linked immunosorbent assay (ELISA) and western blotting demonstrated increased HERVK-Env protein levels in CM from prematurely senescent hMPCs (Figures 5C and S5A), as well as in CM from RS hMPCs (Figures S5B and S5C). Furthermore, through TEM and immuno-TEM analyses, we detected RVLPs with diameters spanning from 80 to 120 nm, primarily on the outside of senescent hMPCs—some HERVK viral particles were detected budding from or adjacent to the cell surface (Figures 5D and S5D), whereas some particles were contained within coated vesicles in the extracellular environment (Figures S5D and S5E).

We next treated young hMPCs (WT) with CM collected from HGPS, WS, or RS hMPCs (referred to as senescent cell-conditional medium or SC-CM), using CM collected from young WT hMPCs as a control. With the TEM analysis, we found that more extracellular RVLPs adhered to the cell surface of young hMPCs or entered the young cells in the SC-CM-treated groups (Figure 5E). After SC-CM treatment, we observed an increased HERVK abundance in young hMPCs (Figure 5F), implying that HERVK in SC-CM may be transmitted into target cells. Moreover, we found that the invaded HERVK elements were associated with an "aging-promoting" effect; that is, young hMPCs that were incubated with SC-CM also underwent accelerated cellular senescence (Figures 5F, 5G, and S5F).

To further investigate whether HERVK present in SC-CM is one of the major factors that causes senescence in young hMPCs, we used an anti-HERVK-Env antibody[56] to immunodeplete HERVK. Western blotting confirmed the pull-down of both HERVK-Env and Gag proteins in SC-CM after incubation with the anti-HERVK-Env antibody but not in SC-CM incubated with the IgG control (Figure S5G). Accordingly, the ELISA data showed the depletion of HERVK-Env from SC-CM after incubation with the anti-HERVK-Env antibody (Figure S5H). As expected, after HERVK immunodepletion, we observed that fewer HERVK RVLPs adhered to the surface or were present in young hMPCs (Figure 5H). Furthermore, the immunodepletion of HERVK resulted in the reduction of HERVK abundance and alleviation of senescence phenotypes in young WT hMPCs compared with those treated with SC-CM without immunodepletion (Figures 5I, S5I, and S5J). Moreover, SC-CM activated the cGAS-STING pathway and induced the expression of SASP genes in young hMPCs (Figures 5F, 5J, and S5K). Importantly, the knockdown of STING rescued the senescent phenotypes induced by SC-CM (Figures 5J, 5K, and S5K), indicating that SC-CM, similar to endogenous HERVK expression, drove cellular senescence at least partially by activating the innate immunity pathway. Collectively, these data suggest that retroviral HERVK elements generated in senescent cells can be released in a paracrine manner and trigger cellular senescence in non-senescent cells.

Next, in order to verify that the infection of extracellular HERVK RVLPs is a direct driver of senescence, we employed our constructed expression vector containing synthesized full-length HERVK with a GFP cassette fused within Env to produce RVLPs (Figures S5L and S5M).[57,58] We then infected young hMPCs with purified HERVK RVLPs (Figures 5L and 5M) and found that both the RNA levels of HERVK and GFP fragments were upregulated in young hMPCs (Figure S5N). Young hMPCs infected with HERVK RVLPs, similar to those treated with SC-CM, showed typical premature senescence phenotypes (Figure 5N), and resembling SC-CM with immunodepletion, HERVK RVLP neutralization with the anti-HERVK-Env antibody abrogated HERVK RVLP-induced cellular senescence (Figures 5O, S5O, and S5P), such abrogation was also achieved by Abacavir treatment (Figures 5P, S5Q, and S5R). We further found an increased enrichment of cGAS on HERVK DNA in recipient hMPCs after infection with HERVK RVLPs (Figure 5Q). Additionally, we also detected the activation of cGAS-STING-mediated innate immune responses in infected hMPCs (Figures 5R, 5S, and S5S). Of note, these phenotypes were abrogated by neutralization with an anti-HERVK-Env antibody or treatment with Abacavir (Figures 5R and 5S), demonstrating that the cGAS-STING pathway drives the acquisition of senescence

(H) TEM analysis of primary human fibroblasts at EP and LP.
(I) qRT-PCR analysis showing the relative expression of HERVK in primary hMPCs from young and old donors.
Scale bars: 10 μm in (A) and (E); 100 and 200 nm (zoomed-in image) in (C), (D), and (H).
See also Figure S2 and Table S2.

Please cite this article in press as: Liu et al., Resurrection of endogenous retroviruses during aging reinforces senescence, Cell (2023), https://doi.org/10.1016/j.cell.2022.12.017

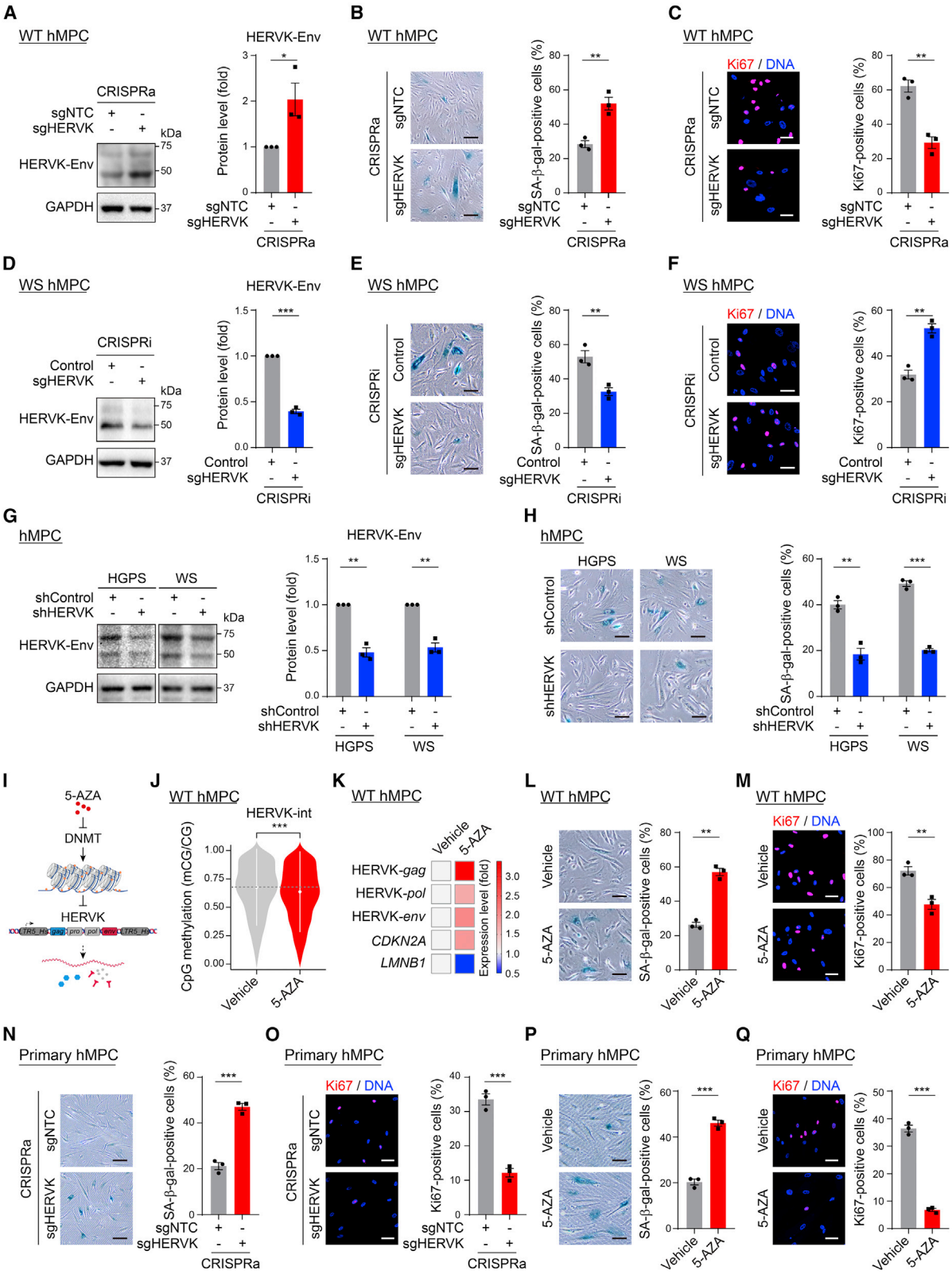

(legend on next page)

Please cite this article in press as: Liu et al., Resurrection of endogenous retroviruses during aging reinforces senescence, Cell (2023), https://doi.org/10.1016/j.cell.2022.12.017

caused by HERVK RVLPs. Taken together, our data support that extracellular HERVK RVLPs transmit aging information to young cells.

Endogenous retrovirus can be used as a biomarker of aging

Next, we measured the levels of endogenous retroviral elements in aged primates and human individuals. ERVW is another endogenous retrovirus subfamily that persists in Old World monkeys due to infection of the ancestral germ line when apes and Old World monkeys diverged about 25 million years ago.[59,60] RT-qPCR results revealed that both ERVK and ERVW elements were increased in aged cynomolgus monkeys (Figure S6A), and with available antibodies,[61] the ERVW-Env protein levels were confirmed to increase in lung, liver, and skin tissues in physiologically aged cynomolgus monkeys relative to younger counterparts (Figures 6A–6C). Consistently, we also found that the innate immune responses in aged monkey tissues were increased, as evidenced by the upregulation of p-RelA (Figure 6B) and SASP factors (Figures S6B–S6D). Furthermore, when comparing lung, liver, and skin tissues isolated from both WT and HGPS cynomolgus monkeys that recapitulated the premature aging phenotypes of HGPS patients,[62] we found that the protein levels of ERVW-Env, along with p-RelA, were also increased in HGPS cynomolgus monkeys (Figures 6D–6F).

Finally, we sought to investigate whether elevated expression of HERVK is observed in human tissues during physiological aging. Likewise, in the skin and serum samples obtained from young and old donors,[63] HERVK-Env expression was markedly increased with age (Figures 6G–6I; Table S2). To ascertain whether HERVK in the serum from old individuals is a factor that drives aging, we cultured young primary hMPCs with a medium that contained serum from young or old individuals (Figure S6E). Strikingly, we found that serum from old individuals increased HERVK abundance, elicited innate immune responses, and accelerated cellular senescence in primary hMPCs, while this pro-senescence capability was abolished upon HERVK immunodepletion (Figures S6F–S6H). Taken together, these results indicate that human endogenous retrovirus HERVK may serve as a potential biomarker to assess human aging as well as a potential therapeutic target for alleviating tissue and cellular senescence.

Targeting endogenous retrovirus alleviates tissue aging

Next, we attempted to inhibit the expression of ERVs in aged mice. Unlike humans, mice harbor a range of active ERVs among which mouse mammary tumor virus (MMTV), is also a known beta retrovirus and is most closely related to that of HERVK (HML-2).[64,65] Similar to the increased levels of ERV elements as we observed in primate and human tissues during aging, MMTV-Env levels were increased in the lung, liver, and skin tissues of aged mice relative to young mice, alongside the activation of the innate immunity and inflammatory pathways therein (Figures S7A–S7C). Thus, with some evolutionary conservation, both primate and rodent ERVs are reactivated during aging.

Articular degeneration, or osteoarthritis (OA), is the most common joint pathology with aging and has been attributed to the senescence of mesenchymal progenitor cells.[66–72] Its pathology is demarcated by decreased numbers of Ki67-positive cells and reduced cartilage thickness (Figures S7D and S7E). In aged mice, we found that MMTV was substantially upregulated in the articular cartilage (Figure 7A), suggesting that increased levels of ERVs could be a potential driver for aging-associated articular degeneration. Consistently, when we performed intra-articular injections of lentivirus carrying CRISPRi-dCas9/sgMMTV (sgRNA targeting MMTV) to repress MMTV (Figures 7B, 7C, and S7F), we detected phenotypes indicative of the alleviation of tissue aging (Figures 7D, 7E, S7G, and S7H). We also observed structural and functional improvements in the joints of aged mice upon MMTV inhibition, as revealed by increased cartilage thickness and joint bone density, as well as enhanced grip strength (Figures 7F, 7G, and S7I).

Our findings that Abacavir treatment can inhibit the senescence-promoting effect of endogenous retrovirus (Figures 4N, 4O, 5P, 5S, S4K, and S5R) lay a foundation for further applying Abacavir to aging intervention *in vivo*. To this end, we performed weekly Abacavir injections into the articular cavities of 22-month-old mice (Figure 7H). Similar to the lentiviral knockdown of MMTV using a CRISPRi system, we found that Abacavir treatment reduced cartilage degeneration, as evidenced by mitigated senescence and attenuated aging-associated inflammation (Figures 7I, 7J, S7J, and S7K). We also detected alleviation of aging-related articular degeneration, including augmented cartilage thickness, bone density, and grip strength (Figures 7K, 7L, and S7L). Finally, we asked whether Abacavir treatment could more generally improve health in aged mice. To this end, we treated 18-month-old mice with Abacavir dissolved in daily drinking water for 6 months (Figure 7M). Strikingly, we detected increased grip strength, improved overall physical score, and improved short-term memory in aged mice that were treated with Abacavir relative to untreated mice (Figures 7N–7P). Taken together, these data indicate that repression of endogenous retrovirus *in vivo* alleviates tissue aging and, to some extent, organismal aging.

Figure 3. Increased HERVK drives senescence

(A–H) Western blotting of HERVK-Env, SA-β-gal, and Ki67 staining of WT hMPCs transduced with lentiviruses expressing sgNTC or sgHERVK using a CRISPRa system (A)–(C), those expressing control or sgHERVK using a CRISPRi system (D)–(F), and those delivering shControl or shHERVK (G) and (H).

(I) Schematic diagram showing the experimental design for activating HERVK with 5-AZA.

(J) Violin plot showing the relative CpG DNA methylation levels for HERVK in WT hMPCs treated with vehicle or 5-AZA.

(K) Heatmap showing the expression levels of HERVK-*gag/pol/env*, *CDKN2A*, and *LMNB1* in WT hMPCs treated with vehicle or 5-AZA by qRT-PCR analysis.

(L–Q) SA-β-gal and Ki67 staining of WT hMPCs treated with vehicle or 5-AZA (L) and (M), of primary hMPCs from a young individual transduced with lentiviruses expressing sgNTC or sgHERVK using the CRISPRa system (N) and (O), and of vehicle- or 5-AZA-treated primary hMPCs from a young individual (P) and (Q). Scale bars, 20 μm (all panels).

See also Figure S3.

Please cite this article in press as: Liu et al., Resurrection of endogenous retroviruses during aging reinforces senescence, Cell (2023), https://doi.org/10.1016/j.cell.2022.12.017

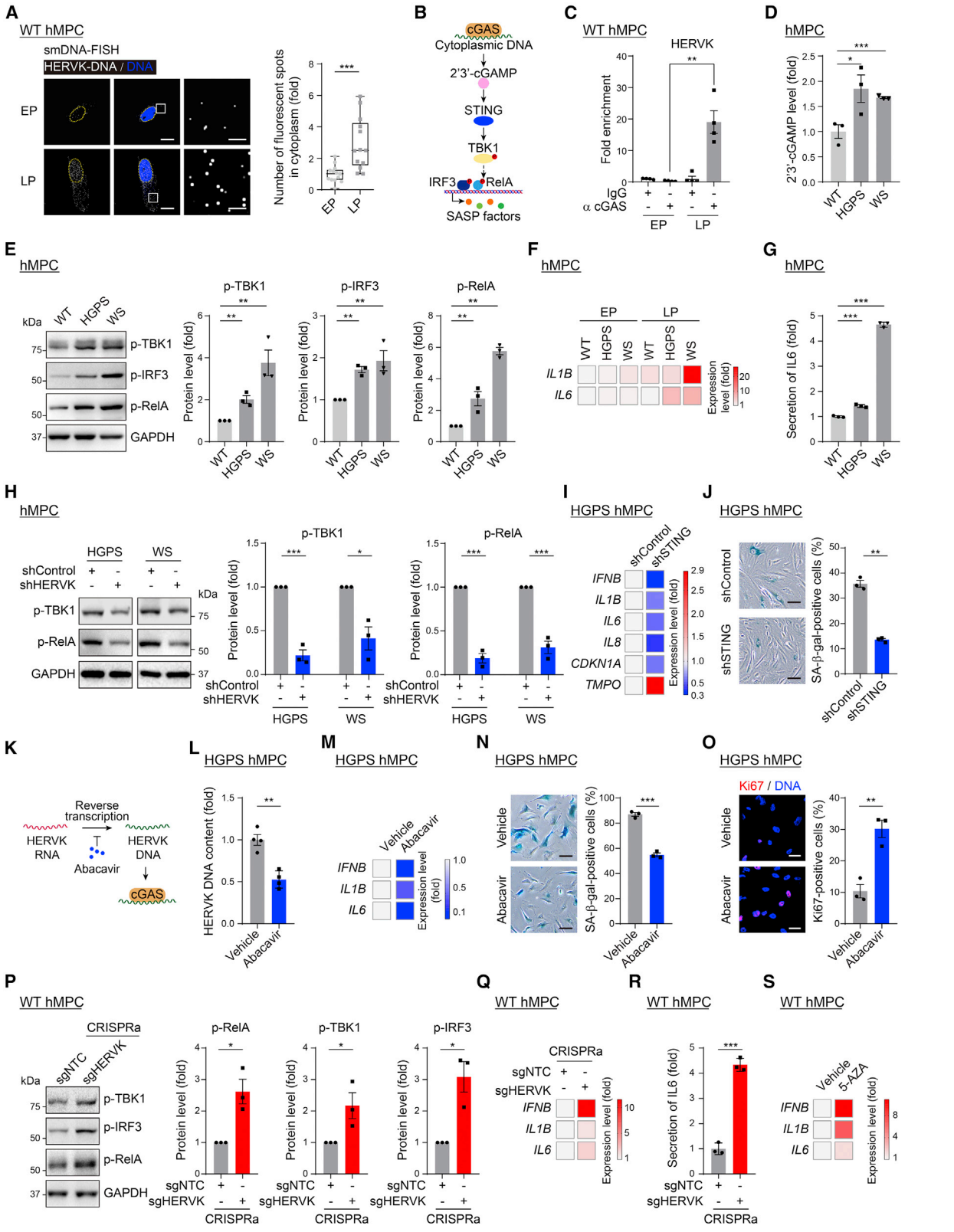

(legend on next page)

Please cite this article in press as: Liu et al., Resurrection of endogenous retroviruses during aging reinforces senescence, Cell (2023), https://doi.org/10.1016/j.cell.2022.12.017

DISCUSSION

In this study, using various primate and rodent aging models, we discovered a positive feedback loop between endogenous retrovirus activation and aging. Our comprehensive analysis unraveled the causal relationship between HERVK and aging in multiple species and was supported by pioneering studies showing increased expression of ERVs concomitant with aging in yeast, fly, and rodent models.[73–75] For instance, the activation of gypsy, a transposable element in *Drosophila* showing homology with vertebrate ERVs, was reported in aged flies.[76] In addition, emerging studies suggested a correlation between awakened ERVs and aging-related disorders, such as rheumatoid arthritis and neurodegenerative diseases.[42,77–81] More importantly, we successfully employed multiple strategies to block the pro-senescence effect of ERVs, demonstrating the alleviation of aging defects across cellular models and multiple tissues *in vivo*. In line with our results, attempts to alleviate neurodegenerative disorders including amyotrophic lateral sclerosis (ALS) via the inhibition of HERVK were reported.[82,83] Thus, ERVs represent druggable targets for alleviating aspects of aging and improving overall organismal health.

As another type of retrotransposon element, LINE1 can also be activated during senescence and age-associated degeneration, and exert certain pro-senescence effects.[8,10,12,84,85] Moreover, inhibition of LINE1 by reverse transcriptase inhibitors has been reported to alleviate aging-related phenotypes and extend the healthspan of mice.[9,11] However, unlike LINE1, which is incapable of producing viral particles and thus acts primarily in a cell-autonomous manner, our study provides evidence that the aging-induced resurrection of endogenous retrovirus (AIR-ERV) not only exerts a devastating cell-autonomous role but also triggers secondary senescence in a paracrine manner.

In summary, our research provides experimental evidence that the conserved activation of ERVs is a hallmark and driving force of cellular senescence and tissue aging. Our findings make fresh insights into understanding aging mechanisms and especially enrich the theory of programmed aging. As such, our work lays the foundation for understanding the contagiousness of aging, opening avenues for establishing a scientific method for evaluating aging and developing clinical strategies to alleviate aging.

Limitations of the study

Although we have provided evidence indicating the transmission process of HERVK RVLPs from senescent cells to young ones, more advanced technologies are required to monitor the exocytosis and endocytosis of viral particles by the donor and recipient cells in real time. It should be noted that a careful decision based on multiple indicators, beyond SA-β-gal activity alone,[86,87] is urgently needed when evaluating HERVK-mediated cellular senescence. In addition, as short-read sequencing cannot be utilized to pinpoint the full-length copy of HERVK, further investigations are necessary to address whether an intact HERVK provirus may exist and how the full life cycle of a HERVK provirus is completed during aging. As we demonstrated the effectiveness of aging alleviation via targeted inhibition of HERVK/MMTV in hMPCs and mice, it will be of great significance to perform preclinical trials in non-human primates for future translational applications. In addition, future studies will be needed to characterize endogenous retrovirus expression profiles across ages and species in large populations and examine the results with other aging clocks, such as DNA methylation and telomere length.

STAR★METHODS

Detailed methods are provided in the online version of this paper and include the following:

- KEY RESOURCES TABLE
- RESOURCE AVAILABILITY
  - Lead Contact
  - Materials Availability
  - Data and Code Availability
- EXPERIMENTAL MODEL AND SUBJECT DETAILS
  - Animals and human samples and ethics
  - Cell culture
- METHOD DETAILS
  - Animal experiments
  - Grip strength test
  - Y maze test

Figure 4. Increased HERVK activates the innate immunity pathway

(A) HERVK smDNA-FISH in RS WT hMPCs.

(B) Schematic diagram showing the innate immune response through the cGAS-STING pathway.

(C) Immunoprecipitation assay followed by qPCR analysis to assess cGAS enrichment on cytoplasmic HERVK DNA fragments in RS WT hMPCs.

(D–G) ELISA analysis of 2′3′-cGAMP levels (D), western blotting of p-TBK1, p-IRF3, and p-RelA (E), qRT-PCR analysis of the levels of SASP genes (F), and ELISA analysis of IL6 levels in the culture medium (G), in WT, HGPS, and WS hMPCs.

(H) Western blotting of p-TBK1 and p-RelA in HGPS or WS hMPCs after transduction with lentiviruses delivering shControl or shHERVK.

(I and J) qRT-PCR analysis of the levels of SASP and senescence marker genes (I), and SA-β-gal staining (J) of HGPS hMPCs after transduction with lentiviruses expressing shControl or shSTING.

(K) Schematic diagram showing the experimental design for repressing HERVK with Abacavir.

(L–O) qPCR analysis of the HERVK DNA contents (L) and qRT-PCR analysis of the expression of SASP genes (M), as well as SA-β-gal (N) and Ki67 (O) staining of HGPS hMPCs treated with vehicle or Abacavir.

(P–R) Western blotting showing the protein levels of p-TBK1, p-IRF3, and p-RelA (P), as well as qRT-PCR analysis of the expression of SASP genes (Q), and ELISA analysis of IL6 levels in the culture medium (R), in WT hMPCs transduced with lentiviruses expressing sgNTC or sgHERVK using a CRISPRa system.

(S) Heatmap showing the qRT-PCR analysis of levels of SASP genes in WT hMPCs treated with vehicle or 5-AZA.

Scale bars: 10 μm and 200 nm (zoomed-in images) in (A); and 20 μm in (J), (N), and (O).

See also Figure S4 and Tables S3 and S4.

Please cite this article in press as: Liu et al., Resurrection of endogenous retroviruses during aging reinforces senescence, Cell (2023), https://doi.org/10.1016/j.cell.2022.12.017

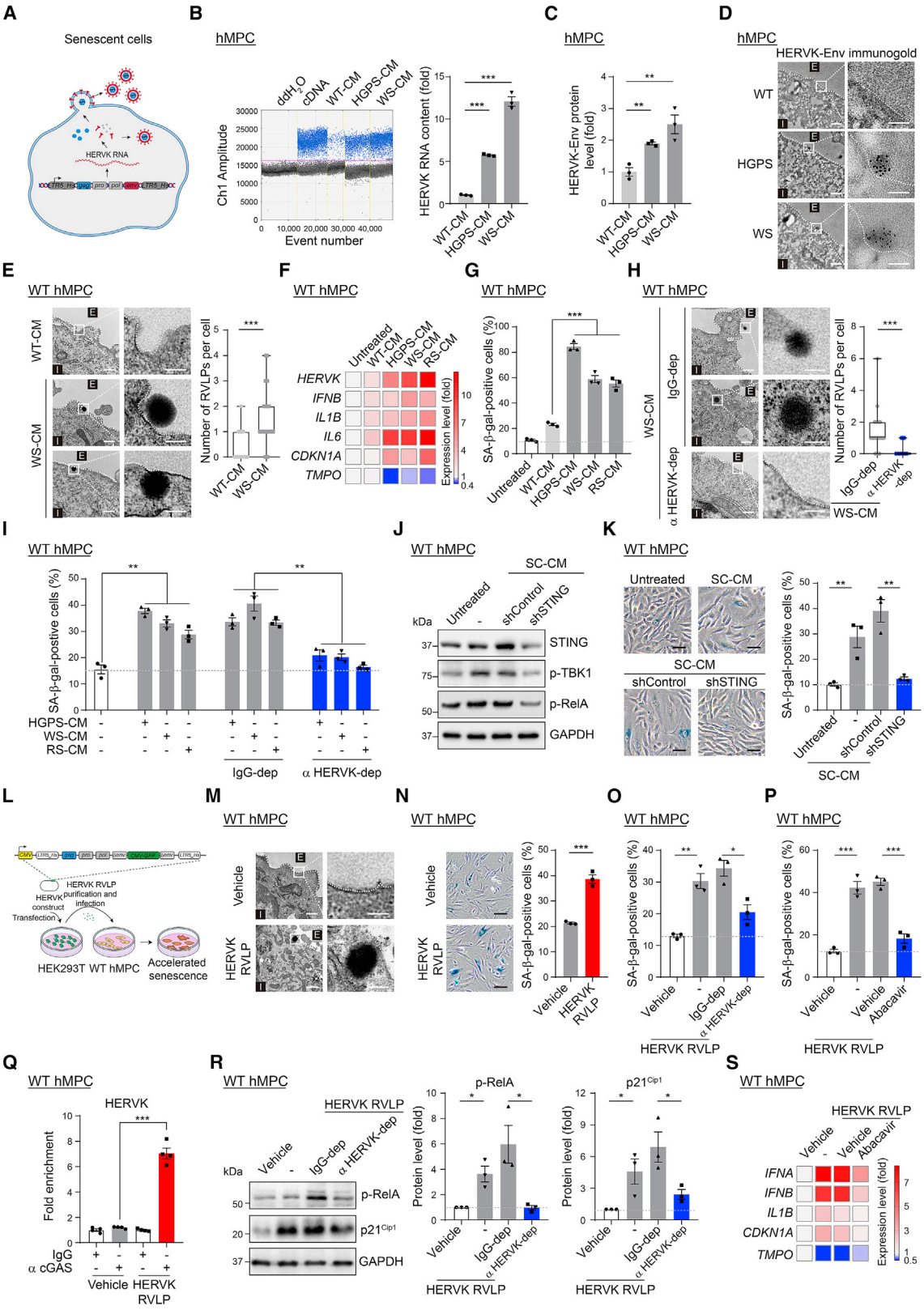

(legend on next page)

- *In vivo* bone histomorphometric analysis: Micro-Computed Tomography (Micro-CT)
- Western blotting
- Immunoprecipitation (IP) of HERVK from conditioned medium
- Purification of microvesicle particles from conditioned medium
- DNA/RNA isolation and quantitative (reverse transcription) PCR (qRT-PCR)
- Viral RNA isolation from microvesicles
- Droplet Digital PCR (ddPCR)
- ELISA
- Immunofluorescence, immunohistochemistry staining and microscopy
- (sm)RNA/DNA-FISH
- (Immuno-)Transmission electron microscopy (TEM)
- Plasmid construction
- Production of HERVK RVLPs and lentiviruses
- Cell treatment
- Clonal expansion assay
- SA-β-gal staining
- ChIP-qPCR
- Strand-specific RNA sequencing (RNA-seq)
- RNA-seq data processing
- Analysis of the expression levels of repetitive elements
- Whole genome bisulfite sequencing (WGBS) library construction and sequencing
- WGBS data processing

● QUANTIFICATION AND STATISTICAL ANALYSIS

SUPPLEMENTAL INFORMATION

Supplemental information can be found online at https://doi.org/10.1016/j.cell.2022.12.017.

ACKNOWLEDGMENTS

We would like to thank the Center for Biological Imaging (CBI), the Institute of Biophysics (Chinese Academy of Science) for TEM analysis, and we are grateful to C. Peng for the TEM sample preparation and L. Zhang for the help with the TEM operation. We would also like to express our gratitude to Y. Li (Tsinghua University) for the immuno-TEM sample preparation. We thank Z. Zhang and Y. Tao (Spatial FISH, Co., Ltd) for the technical help in the FISH experiment, as well as S. Li and J. Hao (the Center of Imaging facility of the Institute of Zoology and Institute of Biophysics [Chinese Academy of Sciences]) for the help with imaging scanning. We would also like to thank Dr. G. Pei for his insightful comments. We are grateful to J. Jia, L. Huang, and W. Wang for their help in animal experiments, as well as L. Bai, Q. Chu, L. Tian, J. Lu, Y. Yang, X. Li, J. Chen, R. Bai, and X. Jing for their administrative assistance. We also would like to thank the Chinese Primate Biomedical Research Alliance (CPBRA), and the Aging Biomarker Consortium, China (ABC) for supporting our study. This work was supported by the National Key R&D Program of China (2020YFA0804000), the Strategic Priority Research Program of the Chinese Academy of Sciences (XDA16000000), the National Key R&D Program of China (2022YFA1103700, 2018YFC2000100, 2018YFA0107203, 2020YFA0112200, 2019YFA0802202, 2020YFA0803401, 2021YFF1201005, 2022YFA1103800, and 2019YFA0110100), the National Natural Science Foundation of China (81921006, 82125011, 92149301, 92168201, 91949209, 92049304, 92049116, 32121001, 82192863, 82122024, 82071588, 31970597, 81861168034, 31900524, 32100937, 32000510, 32200610, and 82201727), the STI2030-Major Projects (2021ZD0202400), the CAS Project for Young Scientists in Basic Research (YSBR-076 and YSBR-012), the Program of the Beijing Natural Science Foundation (Z190019), K. C. Wong Education Foundation (GJTD-2019-06, GJTD-2019-08), the Pilot Project for Public Welfare Development and Reform of Beijing-affiliated Medical Research Institutes (11000022T000000461062), the Youth Innovation Promotion Association of CAS (E1CAZW0401), the Young Elite Scientists Sponsorship Program by CAST (YESS20200012), the Informatization Plan of Chinese Academy of Sciences (CAS-WX2021SF-0301, CAS-WX2022SDC-XK14, and CAS-WX2021SF-0101), and the Tencent Foundation (2021-1045).

AUTHOR CONTRIBUTIONS

G.-H.L., J.Q., and W.Z. conceptualized the work and supervised the overall experiments. X.L. performed the cell culture and the experiments related to functional and mechanistic analyses, including western blotting, qRT-PCR, ddPCR, ChIP-qPCR, and immunofluorescence staining. Z.L. performed bioinformatic analyses. Z.W. performed cell culture and sequencing library construction. J.R. performed the manuscript writing. L.S. provided human serum samples. Y.F. performed immunohistochemistry staining in cynomolgus monkeys and humans. Y.N. provided HGPS cynomolgus monkey samples. G.C. and L.L. performed smRNA/DNA-FISH. X.J. performed fibroblast cell culture and functional analyses. Q.J., Y.E.Z., S.T., and Yingao Cai helped with the bioinformatic analyses. B.Z. performed statistical analysis of immunohistochemistry staining. C.W. performed the cell culture. Q.W. helped with the schematic diagram drawing. K.Y. helped with vector constructions. W.L. organized the animal

Figure 5. HERVK RVLPs released by senescent cells induce senescence in young cells

(A) Schematic diagram showing the proposed HERVK viral life cycle in senescent cells.
(B and C) Digital droplet PCR (ddPCR) analysis of HERVK RNA levels (B) and ELISA analysis of HERVK-Env protein levels (C) in the CM of WT, HGPS, and WS hMPCs.
(D) TEM analysis after immunogold labeling with anti-HERVK-Env antibody in WT, HGPS, and WS hMPCs.
(E) TEM analysis of young hMPCs treated with CM from young WT or senescent WS hMPCs.
(F and G) qRT-PCR analysis of the levels of *HERVK*, senescence marker genes and inflammatory cytokines (F), as well as statistical analysis of SA-β-gal-positive cells (G) in young hMPCs treated with SC-CM.
(H and I) TEM analysis (H) and statistical analysis of SA-β-gal-positive cells (I) in young hMPCs treated with SC-CM after immunodepletion with IgG or anti-HERVK-Env antibody.
(J and K) Western blotting of STING, p-TBK1, and p-RelA (J), as well as SA-β-gal staining (K) in young hMPCs treated with SC-CM after STING knockdown.
(L) Schematic diagram showing the experimental procedure for HERVK RVLP infection of WT hMPCs.
(M–P) TEM images (M) and SA-β-gal staining (N) of WT hMPCs infected with HERVK RVLPs, as well as SA-β-gal staining of WT hMPCs infected with HERVK RVLPs after pretreatment with IgG or anti-HERVK-Env antibody (O), or in the presence of Abacavir (P).
(Q) Immunoprecipitation assay followed by qPCR analysis to assess cGAS enrichment on HERVK DNA fragments in WT hMPCs infected with HERVK RVLPs.
(R) Western blotting of p-RelA and $p21^{Cip1}$ in WT hMPCs infected with HERVK RVLPs after pretreatment with IgG or anti-HERVK-Env antibody.
(S) Heatmap showing the qRT-PCR analysis of the expression levels of inflammatory cytokines and senescence marker genes in WT hMPCs infected with HERVK RVLPs in the presence of Abacavir.
Scale bars: 100 and 200 nm (zoomed-in images) in (D), (E), (H) and (M); and 20 μm in (K) and (N).
See also Figure S5.

Please cite this article in press as: Liu et al., Resurrection of endogenous retroviruses during aging reinforces senescence, Cell (2023), https://doi.org/10.1016/j.cell.2022.12.017

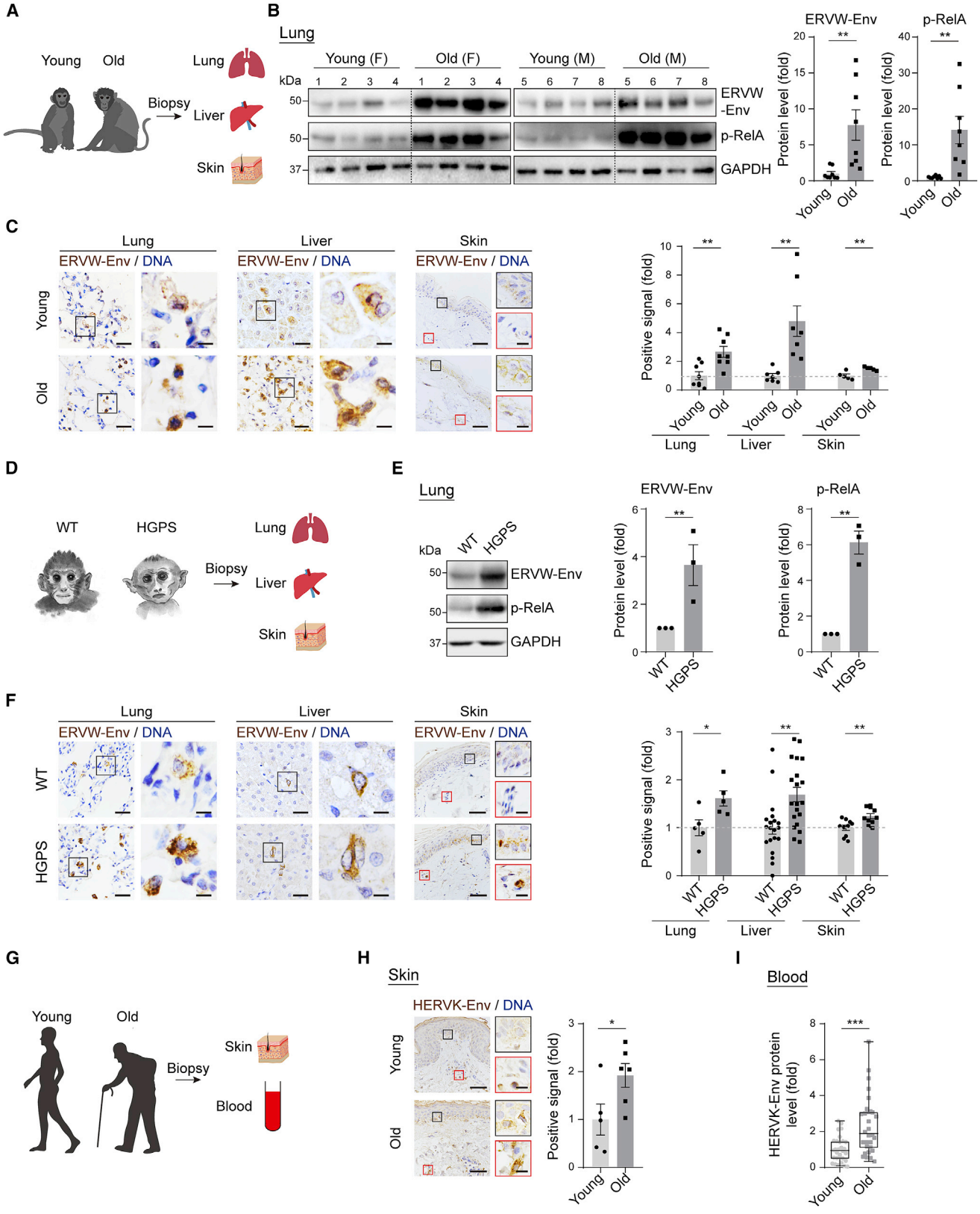

experiments. A.Z. helped with virus purification. W.J., Q.Z., J.C.I.B., C.R.E., F.L., and F.T. helped with supervision of the project. G.-H.L., J.Q., W.Z., J.R., X.L., Z.L., Z.W., Z.J., Yusheng Cai, S.W., and M.S. performed manuscript writing, reviewing, and editing. All authors reviewed the manuscript.

DECLARATION OF INTERESTS

The authors declare no competing interests.

Received: February 24, 2022
Revised: October 13, 2022
Accepted: December 8, 2022
Published: January 6, 2023

REFERENCES

1. Zhang, W., Qu, J., Liu, G.H., and Belmonte, J.C.I. (2020). The ageing epigenome and its rejuvenation. Nat. Rev. Mol. Cell Biol. *21*, 137–150.
2. López-Otín, C., and Kroemer, G. (2021). Hallmarks of health. Cell *184*, 33–63.
3. Horvath, S., and Raj, K. (2018). DNA methylation-based biomarkers and the epigenetic clock theory of ageing. Nat. Rev. Genet. *19*, 371–384.
4. Kennedy, B.K., Berger, S.L., Brunet, A., Campisi, J., Cuervo, A.M., Epel, E.S., Franceschi, C., Lithgow, G.J., Morimoto, R.I., Pessin, J.E., et al. (2014). Geroscience: linking aging to chronic disease. Cell *159*, 709–713.
5. Sun, Y., Li, Q., and Kirkland, J.L. (2022). Targeting senescent cells for a healthier longevity: the roadmap for an era of global aging. Life Med., lnac030. https://doi.org/10.1093/lifemedi/lnac030.
6. Wang, K., Liu, H., Hu, Q., Wang, L., Liu, J., Zheng, Z., Zhang, W., Ren, J., Zhu, F., and Liu, G.H. (2022). Epigenetic regulation of aging: implications for interventions of aging and diseases. Signal Transduct. Target. Ther. *7*, 374.
7. Cai, Y., Song, W., Li, J., Jing, Y., Liang, C., Zhang, L., Zhang, X., Zhang, W., Liu, B., An, Y., et al. (2022). The landscape of aging. Sci. China Life Sci. *65*, 2354–2454.
8. Bi, S., Liu, Z., Wu, Z., Wang, Z., Liu, X., Wang, S., Ren, J., Yao, Y., Zhang, W., Song, M., et al. (2020). SIRT7 antagonizes human stem cell aging as a heterochromatin stabilizer. Protein Cell *11*, 483–504.
9. De Cecco, M., Ito, T., Petrashen, A.P., Elias, A.E., Skvir, N.J., Criscione, S.W., Caligiana, A., Brocculi, G., Adney, E.M., Boeke, J.D., et al. (2019). L1 drives IFN in senescent cells and promotes age-associated inflammation. Nature *566*, 73–78.
10. Liang, C., Ke, Q., Liu, Z., Ren, J., Zhang, W., Hu, J., Wang, Z., Chen, H., Xia, K., Lai, X., et al. (2022). BMAL1 moonlighting as a gatekeeper for LINE1 repression and cellular senescence in primates. Nucleic Acids Res. *50*, 3323–3347.
11. Simon, M., Van Meter, M., Ablaeva, J., Ke, Z., Gonzalez, R.S., Taguchi, T., De Cecco, M., Leonova, K.I., Kogan, V., Helfand, S.L., et al. (2019). LINE1 Derepression in aged wild-type and SIRT6-deficient mice drives inflammation. Cell Metab. *29*, 871–885.e5.
12. Van Meter, M., Kashyap, M., Rezazadeh, S., Geneva, A.J., Morello, T.D., Seluanov, A., and Gorbunova, V. (2014). SIRT6 represses LINE1 retrotransposons by ribosylating KAP1 but this repression fails with stress and age. Nat. Commun. *5*, 5011.
13. Dubnau, J. (2018). The retrotransposon storm and the dangers of a Collyer's genome. Curr. Opin. Genet. Dev. *49*, 95–105.
14. Gorbunova, V., Seluanov, A., Mita, P., McKerrow, W., Fenyö, D., Boeke, J.D., Linker, S.B., Gage, F.H., Kreiling, J.A., Petrashen, A.P., et al. (2021). The role of retrotransposable elements in ageing and age-associated diseases. Nature *596*, 43–53.
15. Liu, B., Qu, J., Zhang, W., Izpisua Belmonte, J.C., and Liu, G.H. (2022). A stem cell aging framework, from mechanisms to interventions. Cell Rep. *41*, 111451.
16. Johnson, W.E. (2019). Origins and evolutionary consequences of ancient endogenous retroviruses. Nat. Rev. Microbiol. *17*, 355–370.
17. Blikstad, V., Benachenhou, F., Sperber, G.O., and Blomberg, J. (2008). Evolution of human endogenous retroviral sequences: a conceptual account. Cell. Mol. Life Sci. *65*, 3348–3365.
18. Subramanian, R.P., Wildschutte, J.H., Russo, C., and Coffin, J.M. (2011). Identification, characterization, and comparative genomic distribution of the HERV-K (HML-2) group of human endogenous retroviruses. Retrovirology *8*, 90.
19. Marchi, E., Kanapin, A., Magiorkinis, G., and Belshaw, R. (2014). Unfixed endogenous retroviral insertions in the human population. J. Virol. *88*, 9529–9537.
20. Stoye, J.P. (2012). Studies of endogenous retroviruses reveal a continuing evolutionary saga. Nat. Rev. Microbiol. *10*, 395–406.
21. Garcia-Montojo, M., Doucet-O'Hare, T., Henderson, L., and Nath, A. (2018). Human endogenous retrovirus-K (HML-2): a comprehensive review. Crit. Rev. Microbiol. *44*, 715–738.
22. Vargiu, L., Rodriguez-Tomé, P., Sperber, G.O., Cadeddu, M., Grandi, N., Blikstad, V., Tramontano, E., and Blomberg, J. (2016). Classification and characterization of human endogenous retroviruses; mosaic forms are common. Retrovirology *13*, 7.
23. Dendrou, C.A., Fugger, L., and Friese, M.A. (2015). Immunopathology of multiple sclerosis. Nat. Rev. Immunol. *15*, 545–558.
24. Sankowski, R., Strohl, J.J., Huerta, T.S., Nasiri, E., Mazzarello, A.N., D'Abramo, C., Cheng, K.F., Staszewski, O., Prinz, M., Huerta, P.T., et al. (2019). Endogenous retroviruses are associated with hippocampus-based memory impairment. Proc. Natl. Acad. Sci. USA *116*, 25982–25990.
25. Mameli, G., Erre, G.L., Caggiu, E., Mura, S., Cossu, D., Bo, M., Cadoni, M.L., Piras, A., Mundula, N., Colombo, E., et al. (2017). Identification of a HERV-K env surface peptide highly recognized in Rheumatoid Arthritis (RA) patients: a cross-sectional case-control study. Clin. Exp. Immunol. *189*, 127–131.
26. Bieda, K., Hoffmann, A., and Boller, K. (2001). Phenotypic heterogeneity of human endogenous retrovirus particles produced by teratocarcinoma cell lines. J. Gen. Virol. *82*, 591–596.
27. Qu, Y., Izsvák, Z., and Wang, J. (2022). Retrotransposon: a versatile player in human preimplantation development and health. Life Med., lnac041. https://doi.org/10.1093/lifemedi/lnac041.
28. Hurst, T.P., and Magiorkinis, G. (2017). Epigenetic control of human endogenous retrovirus expression: focus on regulation of long-terminal repeats (LTRs). Viruses *9*, 130.
29. Tie, C.H., and Rowe, H.M. (2017). Epigenetic control of retrotransposons in adult tissues: implications for immune regulation. Curr. Opin. Virol. *25*, 28–33.

Figure 6. Activation of endogenous retrovirus as a biomarker of aging

(A–F) Schematic diagram of samples (A), western blotting of ERVW-Env and p-RelA in the lungs (B), and immunohistochemistry analysis of ERVW-Env in the lungs, livers, and skin (C) from young and old cynomolgus monkeys or those from WT and HGPS cynomolgus monkeys (D)–(F).
(G–I) Schematic diagram of samples (G), immunohistochemistry analysis of HERVK-Env in the skins (H), and ELISA analysis of HERVK-Env levels in serum (I) from young and old human donors.
Scale bars, 50 and 10 μm (zoomed-in image) (all panels).
See also Figure S6 and Table S2.

Please cite this article in press as: Liu et al., Resurrection of endogenous retroviruses during aging reinforces senescence, Cell (2023), https://doi.org/10.1016/j.cell.2022.12.017

CellPress

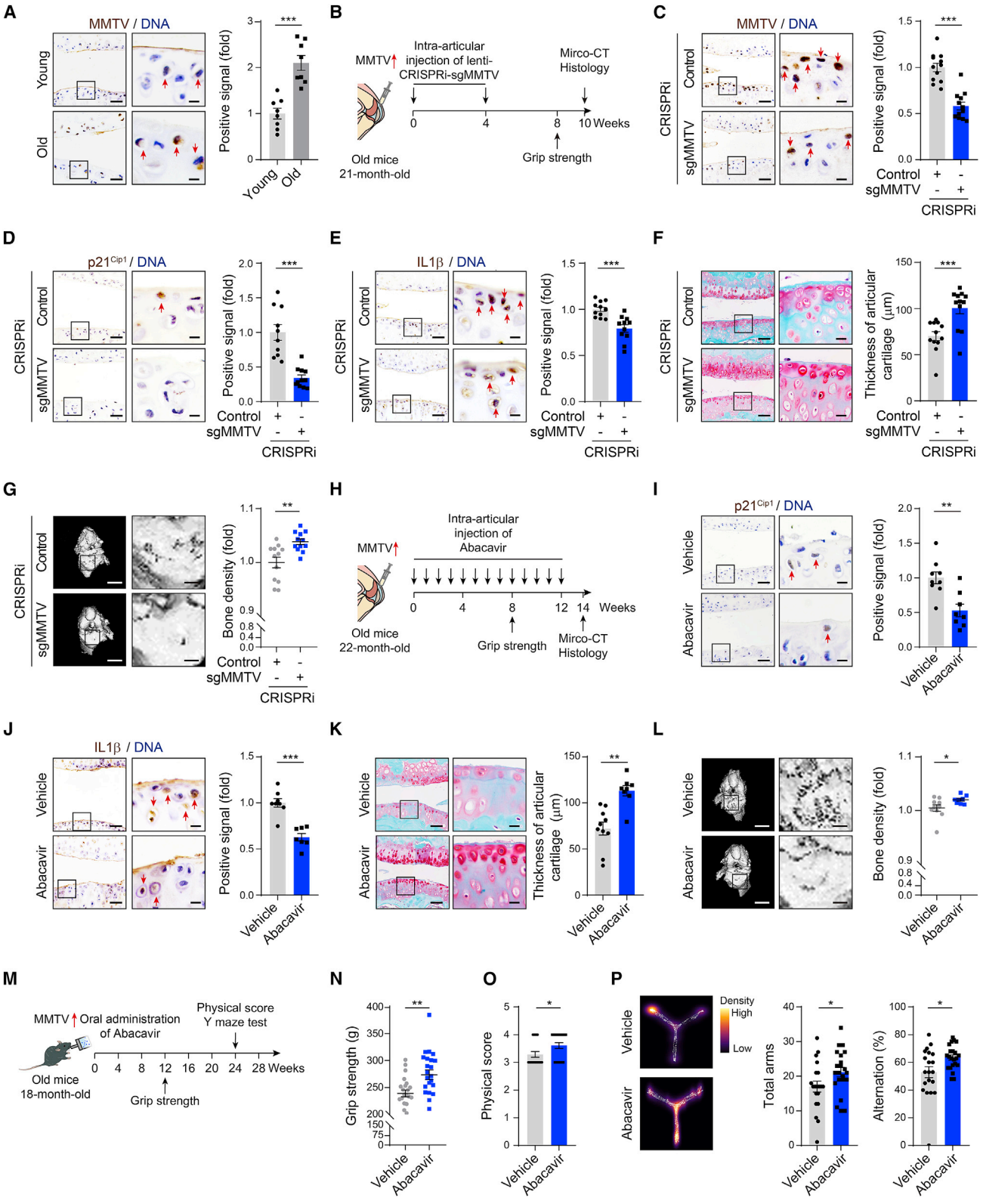

(legend on next page)

30. Kudlow, B.A., Kennedy, B.K., and Monnat, R.J., Jr. (2007). Werner and Hutchinson-Gilford progeria syndromes: mechanistic basis of human progeroid diseases. Nat. Rev. Mol. Cell Biol. *8*, 394–404.

31. Liu, G.H., Barkho, B.Z., Ruiz, S., Diep, D., Qu, J., Yang, S.L., Panopoulos, A.D., Suzuki, K., Kurian, L., Walsh, C., et al. (2011). Recapitulation of premature ageing with iPSCs from Hutchinson-Gilford progeria syndrome. Nature *472*, 221–225.

32. Zhang, W., Li, J., Suzuki, K., Qu, J., Wang, P., Zhou, J., Liu, X., Ren, R., Xu, X., Ocampo, A., et al. (2015). A Werner syndrome stem cell model unveils heterochromatin alterations as a driver of human aging. Science *348*, 1160–1163.

33. Wu, Z., Zhang, W., Song, M., Wang, W., Wei, G., Li, W., Lei, J., Huang, Y., Sang, Y., Chan, P., et al. (2018). Differential stem cell aging kinetics in Hutchinson-Gilford progeria syndrome and Werner syndrome. Protein Cell *9*, 333–350.

34. Geng, L., Liu, Z., Zhang, W., Li, W., Wu, Z., Wang, W., Ren, R., Su, Y., Wang, P., Sun, L., et al. (2019). Chemical screen identifies a geroprotective role of quercetin in premature aging. Protein Cell *10*, 417–435.

35. Li, Y., Zhang, W., Chang, L., Han, Y., Sun, L., Gong, X., Tang, H., Liu, Z., Deng, H., Ye, Y., et al. (2016). Vitamin C alleviates aging defects in a stem cell model for Werner syndrome. Protein Cell *7*, 478–488.

36. Campisi, J., Kapahi, P., Lithgow, G.J., Melov, S., Newman, J.C., and Verdin, E. (2019). From discoveries in ageing research to therapeutics for healthy ageing. Nature *571*, 183–192.

37. Wang, W., Zheng, Y., Sun, S., Li, W., Song, M., Ji, Q., Wu, Z., Liu, Z., Fan, Y., Liu, F., et al. (2021). A genomewide CRISPR-based screen identifies KAT7 as a driver of cellular senescence. Sci. Transl. Med. *13*, eabd2655.

38. Robin, J.D., and Magdinier, F. (2016). Physiological and pathological aging affects chromatin dynamics, structure and function at the nuclear edge. Front. Genet. *7*, 153.

39. Liu, Z., Ji, Q., Ren, J., Yan, P., Wu, Z., Wang, S., Sun, L., Wang, Z., Li, J., Sun, G., et al. (2022). Large-scale chromatin reorganization reactivates placenta-specific genes that drive cellular aging. Dev. Cell *57*, 1347–1368.e12.

40. Zhao, D., and Chen, S. (2022). Failures at every level: breakdown of the epigenetic machinery of aging. Life Med., lnac016. https://doi.org/10.1093/lifemedi/lnac016.

41. Contreras-Galindo, R., Kaplan, M.H., Leissner, P., Verjat, T., Ferlenghi, I., Bagnoli, F., Giusti, F., Dosik, M.H., Hayes, D.F., Gitlin, S.D., et al. (2008). Human endogenous retrovirus K (HML-2) elements in the plasma of people with lymphoma and breast cancer. J. Virol. *82*, 9329–9336.

42. Li, W., Lee, M.H., Henderson, L., Tyagi, R., Bachani, M., Steiner, J., Campanac, E., Hoffman, D.A., von Geldern, G., Johnson, K., et al. (2015). Human endogenous retrovirus-K contributes to motor neuron disease. Sci. Transl. Med. *7*, 307ra153.

43. Turelli, P., Playfoot, C., Grun, D., Raclot, C., Pontis, J., Coudray, A., Thorball, C., Duc, J., Pankevich, E.V., Deplancke, B., et al. (2020). Primate-restricted KRAB zinc finger proteins and target retrotransposons control gene expression in human neurons. Sci. Adv. *6*, eaba3200.

44. Grow, E.J., Flynn, R.A., Chavez, S.L., Bayless, N.L., Wossidlo, M., Wesche, D.J., Martin, L., Ware, C.B., Blish, C.A., Chang, H.Y., et al. (2015). Intrinsic retroviral reactivation in human preimplantation embryos and pluripotent cells. Nature *522*, 221–225.

45. Li, M., Radvanyi, L., Yin, B., Rycaj, K., Li, J., Chivukula, R., Lin, K., Lu, Y., Shen, J., Chang, D.Z., et al. (2017). Downregulation of Human endogenous retrovirus Type K (HERV-K) Viral env RNA in Pancreatic Cancer Cells Decreases Cell Proliferation and Tumor Growth. Clin. Cancer Res. *23*, 5892–5911.

46. Roulois, D., Loo Yau, H., Singhania, R., Wang, Y., Danesh, A., Shen, S.Y., Han, H., Liang, G., Jones, P.A., Pugh, T.J., et al. (2015). DNA-demethylating agents target colorectal cancer cells by inducing viral mimicry by endogenous transcripts. Cell *162*, 961–973.

47. Chiappinelli, K.B., Strissel, P.L., Desrichard, A., Li, H., Henke, C., Akman, B., Hein, A., Rote, N.S., Cope, L.M., Snyder, A., et al. (2017). Inhibiting DNA methylation causes an interferon response in cancer via dsRNA including endogenous retroviruses. Cell *169*, 361.

48. Schoggins, J.W., MacDuff, D.A., Imanaka, N., Gainey, M.D., Shrestha, B., Eitson, J.L., Mar, K.B., Richardson, R.B., Ratushny, A.V., Litvak, V., et al. (2014). Pan-viral specificity of IFN-induced genes reveals new roles for cGAS in innate immunity. Nature *505*, 691–695.

49. Seth, R.B., Sun, L., Ea, C.K., and Chen, Z.J. (2005). Identification and characterization of MAVS, a mitochondrial antiviral signaling protein that activates NF-kappaB and IRF 3. Cell *122*, 669–682.

50. Kong, M., Guo, L., Xu, W., He, C., Jia, X., Zhao, Z., et al. (2022). Aging-associated accumulation of mitochondrial DNA mutations in tumor origin. Life Med, lnac014. https://doi.org/10.1093/lifemedi/lnac014.

51. Takahashi, A., Loo, T.M., Okada, R., Kamachi, F., Watanabe, Y., Wakita, M., Watanabe, S., Kawamoto, S., Miyata, K., Barber, G.N., et al. (2018). Downregulation of cytoplasmic DNases is implicated in cytoplasmic DNA accumulation and SASP in senescent cells. Nat. Commun. *9*, 1249.

52. Watanabe, S., Kawamoto, S., Ohtani, N., and Hara, E. (2017). Impact of senescence-associated secretory phenotype and its potential as a therapeutic target for senescence-associated diseases. Cancer Sci. *108*, 563–569.

53. Tyagi, R., Li, W., Parades, D., Bianchet, M.A., and Nath, A. (2017). Inhibition of human endogenous retrovirus-K by antiretroviral drugs. Retrovirology *14*, 21.

54. Contreras-Galindo, R., Kaplan, M.H., Dube, D., Gonzalez-Hernandez, M.J., Chan, S., Meng, F., Dai, M., Omenn, G.S., Gitlin, S.D., and Markovitz, D.M. (2015). Human endogenous retrovirus Type K (HERV-K) particles package and transmit HERV-K–related sequences. J. Virol. *89*, 7187–7201.

55. Hindson, B.J., Ness, K.D., Masquelier, D.A., Belgrader, P., Heredia, N.J., Makarewicz, A.J., Bright, I.J., Lucero, M.Y., Hiddessen, A.L., Legler, T.C., et al. (2011). High-throughput droplet digital PCR system for absolute quantitation of DNA copy number. Anal. Chem. *83*, 8604–8610.

56. Wang, T., Medynets, M., Johnson, K.R., Doucet-O'Hare, T.T., DiSanza, B., Li, W., Xu, Y., Bagnell, A., Tyagi, R., Sampson, K., et al. (2020). Regulation of stem cell function and neuronal differentiation by HERV-K via mTOR pathway. Proc. Natl. Acad. Sci. USA *117*, 17842–17853.

57. Lee, Y.N., and Bieniasz, P.D. (2007). Reconstitution of an infectious human endogenous retrovirus. PLoS Pathog. *3*, e10.

58. Dewannieux, M., Harper, F., Richaud, A., Letzelter, C., Ribet, D., Pierron, G., and Heidmann, T. (2006). Identification of an infectious progenitor for the multiple-copy HERV-K human endogenous retroelements. Genome Res. *16*, 1548–1556.

Figure 7. Targeting endogenous retrovirus alleviates tissue aging

(A) Immunohistochemistry analysis of MMTV-Env in the articular cartilages of young and old mice.

(B–L) Schematic diagram showing the experimental procedure (B), immunohistochemistry analysis of MMTV-Env, $p21^{Cip1}$, IL1β, and Safranin-O/Fast Green staining of the articular cartilages (C)–(F), as well as micro-CT analysis showing the bone densities of the joints (G) of mice injected with lentiviruses expressing control or sgMMTV into articular cavities using a CRISPRi system, or those of mice intra-articularly injected with vehicle or Abacavir (H)–(L).

(M–P) Schematic diagram showing the experimental procedure (M), grip strength analysis (N), overall physical scores (O), and Y maze analysis (P) of old mice fed with vehicle or Abacavir in the drinking water.

Scale bars: 50 and 10 μm (zoomed-in images) in (A), (C)–(F), and (I)–(K); 500 and 100 μm (zoomed-in images) in (G) and (L).

See also Figure S7.

59. Kim, H.S., Takenaka, O., and Crow, T.J. (1999). Isolation and phylogeny of endogenous retrovirus sequences belonging to the HERV-W family in primates. J. Gen. Virol. *80*, 2613–2619.

60. Stengel, A., Roos, C., Hunsmann, G., Seifarth, W., Leib-Mösch, C., and Greenwood, A.D. (2006). Expression profiles of endogenous retroviruses in Old World monkeys. J. Virol. *80*, 4415–4421.

61. Mayer, J., Meese, E., and Mueller-Lantzsch, N. (1998). Human endogenous retrovirus K homologous sequences and their coding capacity in Old World primates. J. Virol. *72*, 1870–1875.

62. Wang, F., Zhang, W., Yang, Q., Kang, Y., Fan, Y., Wei, J., Liu, Z., Dai, S., Li, H., Li, Z., et al. (2020). Generation of a Hutchinson-Gilford progeria syndrome monkey model by base editing. Protein Cell *11*, 809–824.

63. Zou, Z., Long, X., Zhao, Q., Zheng, Y., Song, M., Ma, S., Jing, Y., Wang, S., He, Y., Esteban, C.R., et al. (2021). A single-cell transcriptomic atlas of human skin aging. Dev. Cell *56*, 383–397.e8.

64. Ruggieri, A., Maldener, E., Sauter, M., Mueller-Lantzsch, N., Meese, E., Fackler, O.T., and Mayer, J. (2009). Human endogenous retrovirus HERV-K(HML-2) encodes a stable signal peptide with biological properties distinct from Rec. Retrovirology *6*, 17.

65. Medstrand, P., and Blomberg, J. (1993). Characterization of novel reverse transcriptase encoding human endogenous retroviral sequences similar to type A and type B retroviruses: differential transcription in normal human tissues. J. Virol. *67*, 6778–6787.

66. Liu, Z., Li, W., Geng, L., Sun, L., Wang, Q., Yu, Y., Yan, P., Liang, C., Ren, J., Song, M., et al. (2022). Cross-species metabolomic analysis identifies uridine as a potent regeneration promoting factor. Cell Discov. *8*, 6.

67. Ren, X., Hu, B., Song, M., Ding, Z., Dang, Y., Liu, Z., Zhang, W., Ji, Q., Ren, R., Ding, J., et al. (2019). Maintenance of nucleolar homeostasis by CBX4 alleviates senescence and osteoarthritis. Cell Rep. *26*, 3643–3656.e7.

68. Fu, L., Hu, Y., Song, M., Liu, Z., Zhang, W., Yu, F.X., Wu, J., Wang, S., Izpisua Belmonte, J.C., Chan, P., et al. (2019). Up-regulation of FOXD1 by YAP alleviates senescence and osteoarthritis. PLoS Biol. *17*, e3000201.

69. Lei, J., Jiang, X., Li, W., Ren, J., Wang, D., Ji, Z., Wu, Z., Cheng, F., Cai, Y., Yu, Z.R., et al. (2022). Exosomes from antler stem cells alleviate mesenchymal stem cell senescence and osteoarthritis. Protein Cell *13*, 220–226.

70. Liang, C., Liu, Z., Song, M., Li, W., Wu, Z., Wang, Z., Wang, Q., Wang, S., Yan, K., Sun, L., et al. (2021). Stabilization of heterochromatin by CLOCK promotes stem cell rejuvenation and cartilage regeneration. Cell Res. *31*, 187–205.

71. Deng, L., Ren, R., Liu, Z., Song, M., Li, J., Wu, Z., Ren, X., Fu, L., Li, W., and Zhang, W. (2019). Stabilizing heterochromatin by DGCR8 alleviates senescence and osteoarthritis. Nat. Commun. *10*, 1–16.

72. Song, M., Belmonte, J.C.I., and Liu, G.H. (2019). Age-related cardiopathies gene editing. Aging (Albany, NY) *11*, 1327–1328.

73. De Cecco, M., Criscione, S.W., Peterson, A.L., Neretti, N., Sedivy, J.M., and Kreiling, J.A. (2013). Transposable elements become active and mobile in the genomes of aging mammalian somatic tissues. Aging (Albany, NY) *5*, 867–883.

74. De Cecco, M., Criscione, S.W., Peckham, E.J., Hillenmeyer, S., Hamm, E.A., Manivannan, J., Peterson, A.L., Kreiling, J.A., Neretti, N., and Sedivy, J.M. (2013). Genomes of replicatively senescent cells undergo global epigenetic changes leading to gene silencing and activation of transposable elements. Aging Cell *12*, 247–256.

75. Patterson, M.N., Scannapieco, A.E., Au, P.H., Dorsey, S., Royer, C.A., and Maxwell, P.H. (2015). Preferential retrotransposition in aging yeast mother cells is correlated with increased genome instability. DNA Repair *34*, 18–27.

76. Li, W., Prazak, L., Chatterjee, N., Grüninger, S., Krug, L., Theodorou, D., and Dubnau, J. (2013). Activation of transposable elements during aging and neuronal decline in Drosophila. Nat. Neurosci. *16*, 529–531.

77. Douville, R., Liu, J., Rothstein, J., and Nath, A. (2011). Identification of active loci of a human endogenous retrovirus in neurons of patients with amyotrophic lateral sclerosis. Ann. Neurol. *69*, 141–151.

78. Barbot, W., Dupressoir, A., Lazar, V., and Heidmann, T. (2002). Epigenetic regulation of an IAP retrotransposon in the aging mouse: progressive demethylation and de-silencing of the element by its repetitive induction. Nucleic Acids Res. *30*, 2365–2373.

79. Balestrieri, E., Pica, F., Matteucci, C., Zenobi, R., Sorrentino, R., Argaw-Denboba, A., Cipriani, C., Bucci, I., and Sinibaldi-Vallebona, P. (2015). Transcriptional activity of human endogenous retroviruses in human peripheral blood mononuclear cells. BioMed Res. Int. *2015*, 164529.

80. Nexø, B.A., Villesen, P., Nissen, K.K., Lindegaard, H.M., Rossing, P., Petersen, T., Tarnow, L., Hansen, B., Lorenzen, T., Hørslev-Petersen, K., et al. (2016). Are human endogenous retroviruses triggers of autoimmune diseases? Unveiling associations of three diseases and viral loci. Immunol. Res. *64*, 55–63.

81. Freimanis, G., Hooley, P., Ejtehadi, H.D., Ali, H.A., Veitch, A., Rylance, P.B., Alawi, A., Axford, J., Nevill, A., Murray, P.G., et al. (2010). A role for human endogenous retrovirus-K (HML-2) in rheumatoid arthritis: investigating mechanisms of pathogenesis. Clin. Exp. Immunol. *160*, 340–347.

82. Garcia-Montojo, M., Fathi, S., Norato, G., Smith, B.R., Rowe, D.B., Kiernan, M.C., Vucic, S., Mathers, S., van Eijk, R.P.A., Santamaria, U., et al. (2021). Inhibition of HERV-K (HML-2) in amyotrophic lateral sclerosis patients on antiretroviral therapy. J. Neurol. Sci. *423*, 117358.

83. Gold, J., Rowe, D.B., Kiernan, M.C., Vucic, S., Mathers, S., van Eijk, R.P.A., Nath, A., Garcia Montojo, M., Norato, G., Santamaria, U.A., et al. (2019). Safety and tolerability of Triumeq in amyotrophic lateral sclerosis: the Lighthouse trial. Amyotroph. Lateral Scler. Frontotemporal Degener. *20*, 595–604.

84. Garcia-Perez, J.L., Morell, M., Scheys, J.O., Kulpa, D.A., Morell, S., Carter, C.C., Hammer, G.D., Collins, K.L., O'Shea, K.S., Menendez, P., et al. (2010). Epigenetic silencing of engineered L1 retrotransposition events in human embryonic carcinoma cells. Nature *466*, 769–773.

85. Liu, E.Y., Russ, J., Cali, C.P., Phan, J.M., Amlie-Wolf, A., and Lee, E.B. (2019). Loss of nuclear TDP-43 is associated with decondensation of LINE retrotransposons. Cell Rep. *27*, 1409–1421.e6.

86. Yegorov, Y.E., Akimov, S.S., Hass, R., Zelenin, A.V., and Prudovsky, I.A. (1998). Endogenous beta-galactosidase activity in continuously nonproliferating cells. Exp. Cell Res. *243*, 207–211.

87. Imai, Y., Takahashi, A., Hanyu, A., Hori, S., Sato, S., Naka, K., Hirao, A., Ohtani, N., and Hara, E. (2014). Crosstalk between the Rb pathway and AKT signaling forms a quiescence-senescence switch. Cell Rep. *7*, 194–207.

88. Ma, S., Sun, S., Li, J., Fan, Y., Qu, J., Sun, L., Wang, S., Zhang, Y., Yang, S., Liu, Z., et al. (2021). Single-cell transcriptomic atlas of primate cardiopulmonary aging. Cell Res. *31*, 415–432.

89. Li, H., Handsaker, B., Wysoker, A., Fennell, T., Ruan, J., Homer, N., Marth, G., Abecasis, G., and Durbin, R.; 1000 Genome Project Data Processing Subgroup (2009). The Sequence Alignment/Map format and SAMtools. Bioinformatics *25*, 2078–2079.

90. Subramanian, A., Kuehn, H., Gould, J., Tamayo, P., and Mesirov, J.P. (2007). GSEA-P: a desktop application for Gene Set Enrichment Analysis. Bioinformatics *23*, 3251–3253.

91. Chen, S., Zhou, Y., Chen, Y., and Gu, J. (2018). fastp: an ultra-fast all-in-one FASTQ preprocessor. Bioinformatics *34*, i884–i890.

92. Kim, D., Langmead, B., and Salzberg, S.L. (2015). HISAT: a fast spliced aligner with low memory requirements. Nat. Methods *12*, 357–360.

93. Anders, S., Pyl, P.T., and Huber, W. (2015). HTSeq—a Python framework to work with high-throughput sequencing data. Bioinformatics *31*, 166–169.

94. Liao, Y., Smyth, G.K., and Shi, W. (2014). featureCounts: an efficient general purpose program for assigning sequence reads to genomic features. Bioinformatics *30*, 923–930.

95. Dobin, A., Davis, C.A., Schlesinger, F., Drenkow, J., Zaleski, C., Jha, S., Batut, P., Chaisson, M., and Gingeras, T.R. (2013). STAR: ultrafast universal RNA-seq aligner. Bioinformatics *29*, 15–21.

96. Jin, Y., Tam, O.H., Paniagua, E., and Hammell, M. (2015). TEtranscripts: a package for including transposable elements in differential expression analysis of RNA-seq datasets. Bioinformatics *31*, 3593–3599.

97. Love, M.I., Huber, W., and Anders, S. (2014). Moderated estimation of fold change and dispersion for RNA-seq data with DESeq2. Genome Biol. *15*, 550.

98. Xi, Y., and Li, W. (2009). BSMAP: whole genome bisulfite sequence MAPping program. BMC Bioinformatics *10*, 232.

99. Thorvaldsdóttir, H., Robinson, J.T., and Mesirov, J.P. (2013). Integrative Genomics Viewer (IGV): high-performance genomics data visualization and exploration. Brief. Bioinform. *14*, 178–192.

100. Schneider, C.A., Rasband, W.S., and Eliceiri, K.W. (2012). NIH Image to ImageJ: 25 years of image analysis. Nat. Methods *9*, 671–675.

101. Zhang, W., Zhang, S., Yan, P., Ren, J., Song, M., Li, J., Lei, J., Pan, H., Wang, S., Ma, X., et al. (2020). A single-cell transcriptomic landscape of primate arterial aging. Nat. Commun. *11*, 2202.

102. Li, J., Zheng, Y., Yan, P., Song, M., Wang, S., Sun, L., Liu, Z., Ma, S., Izpisua Belmonte, J.C., Chan, P., et al. (2021). A single-cell transcriptomic atlas of primate pancreatic islet aging. Natl. Sci. Rev. *8*, nwaa127.

103. Balaj, L., Lessard, R., Dai, L., Cho, Y.J., Pomeroy, S.L., Breakefield, X.O., and Skog, J. (2011). Tumour microvesicles contain retrotransposon elements and amplified oncogene sequences. Nat. Commun. *2*, 180.

104. Hu, H., Ji, Q., Song, M., Ren, J., Liu, Z., Wang, Z., Liu, X., Yan, K., Hu, J., Jing, Y., et al. (2020). ZKSCAN3 counteracts cellular senescence by stabilizing heterochromatin. Nucleic Acids Res. *48*, 6001–6018.

105. Padmanabhan Nair, V., Liu, H., Ciceri, G., Jungverdorben, J., Frishman, G., Tchieu, J., Cederquist, G.Y., Rothenaigner, I., Schorpp, K., Klepper, L., et al. (2021). Activation of HERV-K(HML-2) disrupts cortical patterning and neuronal differentiation by increasing NTRK3. Cell Stem Cell *28*, 1566–1581.e8.

106. Nair, V.P., Mayer, J., and Vincendeau, M. (2022). A protocol for CRISPR-mediated activation and repression of human endogenous retroviruses in human pluripotent stem cells. Star Protoc. *3*, 101281. https://doi.org/10.1016/j.xpro.2022.101281.

107. Dewannieux, M., Blaise, S., and Heidmann, T. (2005). Identification of a functional envelope protein from the HERV-K family of human endogenous retroviruses. J. Virol. *79*, 15573–15577.

108. Segel, M., Lash, B., Song, J., Ladha, A., Liu, C.C., Jin, X., Mekhedov, S.L., Macrae, R.K., Koonin, E.V., and Zhang, F. (2021). Mammalian retrovirus-like protein PEG10 packages its own mRNA and can be pseudotyped for mRNA delivery. Science *373*, 882–889.

109. Debacq-Chainiaux, F., Erusalimsky, J.D., Campisi, J., and Toussaint, O. (2009). Protocols to detect senescence-associated beta-galactosidase (SA-betagal) activity, a biomarker of senescent cells in culture and in vivo. Nat. Protoc. *4*, 1798–1806.

110. Kaufmann, K., Muiño, J.M., Østerås, M., Farinelli, L., Krajewski, P., and Angenent, G.C. (2010). Chromatin immunoprecipitation (ChIP) of plant transcription factors followed by sequencing (ChIP-SEQ) or hybridization to whole genome arrays (ChIP-CHIP). Nat. Protoc. *5*, 457–472.

111. Yan, P., Liu, Z., Song, M., Wu, Z., Xu, W., Li, K., Ji, Q., Wang, S., Liu, X., Yan, K., et al. (2020). Genome-wide R-loop Landscapes during Cell Differentiation and Reprogramming. Cell Rep. *32*, 107870. https://doi.org/10.1016/j.celrep.2020.107870.

Please cite this article in press as: Liu et al., Resurrection of endogenous retroviruses during aging reinforces senescence, Cell (2023), https://doi.org/10.1016/j.cell.2022.12.017

STAR★METHODS

KEY RESOURCES TABLE

REAGENT or RESOURCE	SOURCE	IDENTIFIER
Antibodies		
Mouse monoclonal anti-HERVK-Env	Austral Biologicals	Cat# HERM-1811-5; RRID: AB_10891119
Mouse monoclonal anti-HERVK-Gag	Austral Biologicals	Cat# HERM-1841-5; RRID: AB_10891407
Rabbit polyclonal anti-ERVK7	United States Biological	Cat# 302427 RRID: N/A
Rabbit polyclonal anti-ERVW-1	Abcam	Cat# ab179693; RRID: N/A
Rabbit anti-phospho-TBK1/NAK (Ser172)	Cell Signaling Technology	Cat# 5483; RRID: AB_10693472
Rabbit anti-phospho-NF-κB p65 (p-RelA) (Ser536) (93H1)	Cell Signaling Technology	Cat# 3033S; RRID: AB_331284
Rabbit anti-phospho-IRF-3 (Ser396)	Cell Signaling Technology	Cat# 29047S; RRID: AB_2773013
Mouse monoclonal anti-STING	R&D systems	Cat#MAB7169; RRID: AB_10971940
Mouse monoclonal anti-$p16^{INK4a}$	BD Biosciences	Cat# 550834; RRID: AB_2078446
Mouse anti-LAP2	BD Biosciences	Cat# 611000; RRID: AB_398313
Rabbit monoclonal anti-$p21^{Cip1}$	Cell Signaling Technology	Cat# 2947s; RRID: AB_823586
Rabbit monoclonal anti-$p21^{Cip1}$	Abcam	Cat# ab188224; RRID: AB_2734729
Mouse monoclonal anti-GAPDH	Santa Cruz Biotechnology	Cat#; sc-365062; RRID: AB_10847862
Mouse monoclonal anti-β-Actin	Santa Cruz Biotechnology	Cat# sc-69879; RRID: AB_1119529
Rabbit polyclonal anti-H3K9me3	Abcam	Cat# ab8898; RRID: AB_1119529
Rabbit polyclonal anti-H3K36me3	Abcam	Cat# ab9050; RRID: AB_306966
Mouse monoclonal anti-Ki67	ZSGB-Bio	Cat# ZM-0166; RRID: AB_2890067
Rabbit polyclonal anti-Ki67	Abcam	Cat# ab15580; RRID: AB_443209
Rabbit monoclonal anti-cGAS (D1D3G)	Cell Signaling Technology	Cat# 15102S; RRID: AB_2732795
Rabbit polyclonal anti-MMTV-Env	Novus Biologicals, LLC	Cat# NBP2-44179; RRID: N/A
Mouse monoclonal anti-IL1β	Santa Cruz Biotechnology	Cat# sc-52012; RRID: AB_629741
Normal Rabbit IgG	Cell Signaling Technology	Cat# 2729S; RRID: AB_1031062
Normal Mouse IgG	Santa Cruz Biotechnology	Cat# sc-2025; RRID: AB_737182
Alexa Fluo™ 568 Donkey Anti-Rabbit IgG (H+L)	Invitrogen	Cat# A10042; RRID: AB_2534017

(*Continued on next page*)

Please cite this article in press as: Liu et al., Resurrection of endogenous retroviruses during aging reinforces senescence, Cell (2023), https://doi.org/10.1016/j.cell.2022.12.017

Continued

REAGENT or RESOURCE	SOURCE	IDENTIFIER
Alexa Fluo™ 568 Donkey Anti-Mouse IgG (H+L)	Invitrogen	Cat# A-10037; RRID: AB_2534013
Alexa Fluor™ 488 Donkey Anti-Mouse IgG (H+L)	Invitrogen	Cat# A21202; RRID: AB_141607
HRP-conjugated Goat Anti-Mouse IgG (H+L)	ZSGB-Bio	Cat# ZB2305; RRID: AB_2747415
HRP-conjugated Goat Anti-Rabbit IgG (H+L)	ZSGB-Bio	Cat# ZB2301; RRID: AB_2747412
6-nm Gold-labeled Goat Anti-Mouse IgG (H+L)	Jackson ImmunoResearch	Cat# 115-195-146 RRID: N/A
Biological samples		
The young and old cynomolgus monkey tissues	Xieerxin Biology Resource	N/A
The WT and HGPS cynomolgus monkey tissues	Yunnan Key Laboratory of Primate Biomedical Research	N/A
Human eyelid skin samples	Peking Union Medical College Hospital	N/A
Human serum samples	The First Hospital of Kunming Medical University	N/A
Chemicals, peptides, and recombinant proteins		
MEMα	GIBCO	Cat# 32571-101
DMEM/High Glucose	HyClone	Cat# SH30243.01
Non-essential amino acids (NEAA)	GIBCO	Cat# 11140076
Fetal bovine serum (FBS)	GIBCO	Cat# 42Q7980K
Penicillin/streptomycin (P/S)	GIBCO	Cat# 15140-163
GlutaMAX	GIBCO	Cat# 35050079
Gelatin	Sigma-Aldrich	Cat# V900863
bFGF	Joint Protein Central	Cat# BBI-EXP-002
TrypLE Express Enzyme (1X), no phenol red	GIBCO	Cat# 12605010
0.25% Trypsin-EDTA (1X), Phenol Red	GIBCO	Cat# 25200072
Hoechst 33342	Thermo Fisher Scientific	Cat# H3570
THUNDERBIRD SYBR qPCR mix	TOYOBO	Cat# QPS-201(-)
4% paraformaldehyde, PFA	Dingguo, China	Cat# AR-0211
Triton X-100	Sigma-Aldrich	Cat# T9284
Crystal violet	Biohao Biotechnology Co., Ltd., China	Cat# C0502
TRIzol™ Reagent	Thermo Fisher Scientific	Cat# 15596018
DMSO	Sigma-Aldrich	Cat# D2650
NP-40	Dingguo, China	Cat# DH218
Proteinase K	New England Biolabs	Cat# P8107S
RNase A	TAKARA	Cat# 2158
EDTA	Sigma-Aldrich	Cat# EDS-500G
Protease inhibitor cocktail	Roche	Cat# 4693159001
X-gal	Amresca	Cat# 0428-25G
PVDF membranes	Millipore	Cat# IPVH00010
Protein A/G Plus-Agarose	Thermo Fisher Scientific	Cat# sc-2003
QX200 ddPCR EvaGreen Supermix	Bio-Rad Laboratories, Inc.	Cat# 186-4033

(*Continued on next page*)

Please cite this article in press as: Liu et al., Resurrection of endogenous retroviruses during aging reinforces senescence, Cell (2023), https://doi.org/10.1016/j.cell.2022.12.017

Continued

REAGENT or RESOURCE	SOURCE	IDENTIFIER
QX200™ Droplet Generation Oil for EvaGreen	Bio-Rad Laboratories, Inc.	Cat# 1864005
MluI	New England Biolabs	Cat# R0198S
ClaI	New England Biolabs	Cat# R0197S
ESP3I/BsmB1	FERMENTAS	Cat# FD0454
NheI	New England Biolabs	Cat# R3131S
ApaI	New England Biolabs	Cat# R0114S
KpnI-HF	New England Biolabs	Cat# R3142
BamHI-HF	New England Biolabs	Cat# R3136
5-AZA	Sigma-Aldrich	Cat# 320-67-2
Abacavir	Selleckchem	Cat# S3165
Polybrene	Sigma-Aldrich	Cat# 107689
Critical commercial assays		
BCA Protein Assay Kit	Dingguo, China	Cat# BCA02
Qubit™ dsDNA HS Assay Kit	Thermo Fisher Scientific	Cat# Q32854
Dynabeads™ Protein A	Thermo Fisher Scientific	Cat# 10002D
Ribo-Zero™ rRNA Removal Kit	Epicentre Biotechnologies	Cat# RZH1046
NEBNext® Ultra™ Directional RNA Library Prep Kit for Illumina®	New England Biolabs	Cat# E7420L
DNeasy Blood & Tissue Kit	QIAGEN	Cat# 69506
GoScript Reverse Transcription System	Promega	Cat# A5001
Lipofectamine 3000 Transfection Reagent	Thermo Fisher Scientific	Cat# L3000015
QIAamp Viral RNA Mini Kit	QIAGEN	Cat# 52904
SuperSignal™ West Femto Maximum Sensitivity Substrate	Thermo Fisher Scientific	Cat# 34096
TURBO DNA-free™ Kit	Thermo Fisher Scientific	Cat# AM1907
Human IL6 ELISA Kit	BioLegend	Cat# 430515
Human HERVK-Env Polyprotein ELISA Kit	CUSABIO	Cat# CBS-EL007812HU
2'3'-cGAMP ELISA Kit	Cayman	Cat# 501700
DAB Staining Kit	ZSGB-BIO	Cat# ZLI-9018; PV-9001; PV-9002
QuantiGene® ViewRNA ISH Cell Assay Kit	Thermo Fisher Scientific	Cat# QVC0001
Cellular Senescence Detection Kit-SPiDER-βGal	DOJINDO Laboratories	Cat# PL507
Deposited data		
The raw RNA-seq data for prematurely senescent and RS hMPCs	This study	CRA003282
The raw WGBS data for prematurely senescent and RS hMPCs	Liu et al.[39]	HRA001144
The raw WGBS data for vehicle or 5-AZA treated hMPCs	This study	HRA001879
The raw RNA-seq data for WT MPCs (P6) after transduction of lentiviruses with sgRNA targeting HERVK or NTC using a CRISPRa system	This study	CRA003283
The RNA-seq raw data for liver tissues of young and old cynomolgus monkeys	Liu et al.[66]	CRA002965
The RNA-seq raw data for lung tissues of young and old cynomolgus monkeys	Ma et al.[88]	CRA002810

(*Continued on next page*)

Please cite this article in press as: Liu et al., Resurrection of endogenous retroviruses during aging reinforces senescence, Cell (2023), https://doi.org/10.1016/j.cell.2022.12.017

Continued

REAGENT or RESOURCE	SOURCE	IDENTIFIER
Experimental models: Cell lines		
WT hMPCs (derived from WT hESCs (Line H9))	Wu et al.[33]	N/A
LMNA$^{G608G/+}$ hMPCs	Wu et al.[33]	N/A
WRN$^{-/-}$ hMPCs	Zhang et al., Wu et al.[32,33]	N/A
Primary hMPCs were isolated from the gingiva of the individuals	Ren et al.[67]	N/A
HEK293T	ATCC	N/A
Human primary dermal fibroblasts	Zou et al.[63]	N/A
Experimental models: Organisms/strains		
C57BL/6J mice	SiPeiFu (Beijing) Biotechnology Co., Ltd.	N/A
Oligonucleotides		
Primers for qRT-PCR, ChIP-qPCR, and vector constructions, as well as probes for DNA/RNA-FISH, see Table S5	This study	N/A
Recombinant DNA		
pLVTHM	A gift from Didier Trono	Addgene plasmid #12247
psPAX2	A gift from Didier Trono	Addgene plasmid #12260
pMD2.G	A gift from Didier Trono	Addgene plasmid #12259
lentiSAM v2	A gift from Didier Trono	Addgene plasmid #75112
lentiMPH v2	A gift from Didier Trono	Addgene plasmid #89308
dCas9-KRAB	A gift from Didier Trono	N/A
HERVK RVLP construct	This study	N/A
Software and algorithms		
ImageJ (version 1.8.0)	Schneider et al.[100]	https://imagej.net/Welcome
Leica LAS AF Lite (version 2.6.0)	Leica	https://leica-las-af-lite.updatestar.com/
GraphPadPrism 8.0	GraphPad Software Inc.	https://www.graphpad.com/
Image Lab 4.0.1	Bio-Rad	https://www.bio-rad.com/zh-cn/product/imagelab-software?ID=KRE6P5E8Z
Phenochart™ 1.0	Phenochart	https://www.akoyabio.com/support/software/phenochart-whole-slide-viewer/
ImageScope (version 12.3.0.5056)	Leica	https://www.leicabiosystems.com/en-de/digital-pathology/manage/aperio-imagescope/
IMARIS 9.8	OXFORD INSTRUMENTs	https://imaris.oxinst.cn/newrelease
ZEN 3.1	ZEISS	https://www.micro-shop.zeiss.com/en/us/system/zen+software/software+zen/zen+-+basic+software/410135-1002-310
Analyze 10.0	AnalyzeDirect	https://www.analyzedirect.com
TrimGalore (version 0.4.5)	Babraham Bioinformatics	https://github.com/FelixKrueger/TrimGalore
SAMtools (version 1.6)	Li et al.[89]	https://github.com/samtools/samtools
R (version 4.0.2)	N/A	https://www.r-project.org/
pheatmap (version 1.0.12)	N/A	https://cran.r-project.org/web/packages/pheatmap/
ggplot2 (version 3.3.2)	N/A	https://cran.r-project.org/web/packages/ggplot2/

(*Continued on next page*)

Continued

REAGENT or RESOURCE	SOURCE	IDENTIFIER
GSEA (version 4.1)	Subramanian et al.[90]	http://software.broadinstitute.org/gsea/index.jsp
Fastp (version 0.19.10)	Chen et al.[91]	https://github.com/OpenGene/fastp
hisat2 (version 2.0.4)	Kim et al.[92]	https://ccb.jhu.edu/software/hisat2/index.shtml
HTSeq (version 0.11.0)	Anders et al.[93]	https://htseq.readthedocs.io/en/master/
featureCounts (version 2.0.0)	Liao et al.[94]	http://subread.sourceforge.net/featureCounts.html
STAR (version 2.7.1b and 2.7.9a)	Dobin et al.[95]	https://github.com/alexdobin/STAR
TEtranscripts (version 2.2.1)	Jin et al.[96]	https://github.com/mhammell-laboratory/TEtranscripts
DESeq2 (version 1.29.8 and 1.26.0)	Love et al.[97]	https://bioconductor.org/packages/release/bioc/html/DESeq2.html
bsmap (version 2.90)	Xi and Li[98]	https://hpc.nih.gov/apps/bsmap.html
ggpubr (version 0.4.0)	N/A	https://cran.microsoft.com/snapshot/2021-09-26/web/packages/ggpubr/index.html
IGV (version 2.8.12)	Thorvaldsdottir et al.[99]	https://igv.org

RESOURCE AVAILABILITY

Lead Contact

Further information and requests for resources and reagents should be directed to and will be fulfilled by the lead contact Dr. Guang-Hui Liu (ghliu@ioz.ac.cn).

Materials Availability

This study did not generate new unique reagents.

Data and Code Availability

All datasets have been deposited in the Genome Sequence Archive in the National Genomics Data Center with accession numbers as indicated. The raw RNA-seq data for prematurely senescent and RS hMPCs: CRA003282. The raw WGBS data for prematurely senescent and RS hMPCs: HRA001144.[39] The raw WGBS data for vehicle or 5-AZA treated hMPCs: HRA001879. The raw RNA-seq data for WT hMPCs (P6) after transduction with lentivirus containing sgRNA targeting HERVK or NTC using a CRISPRa system: CRA003283. The RNA-seq raw data for liver tissues of young and old cynomolgus monkeys: CRA002965.[66] The RNA-seq raw data for lung tissues of young and old cynomolgus monkeys: CRA002810.[88] Any additional information required to reanalyze the data reported in this work is available from the lead contact upon request.

EXPERIMENTAL MODEL AND SUBJECT DETAILS

Animals and human samples and ethics

C57BL/6J mice purchased from SiPeiFu (Beijing) Biotechnology Co., Ltd, were maintained in the animal care facilities of Institute of Biophysics and Institute of Zoology, Chinese Academy of Sciences, and fed *ad libitum* with standard laboratory chow and water in ventilated cages under a 12 h light/dark cycle. All mouse experiments followed the Principles for the Application Format for Ethical Approval for Research Involving Animals and were approved in advance by the Institutional Animal Care and Use Committee of the Institute of Zoology, Chinese Academy of Sciences. Anaesthetization of mice was conducted with isoflurane and euthanization was performed with CO_2 followed by cervical dislocation. All cynomolgus monkey experiments were conducted under the Principles for the Ethical Treatment of Non-Human Primates and approved by the Animal Care and Ethics Committee of Institute of Zoology, Chinese Academy of Sciences. The young and old cynomolgus monkeys used for the experiments were raised at the Xieerxin Biology Resource with accreditation by a Laboratory Animal Care accredited facility in Beijing, in compliance with all local and federal laws governing animal research.[101] The cynomolgus monkeys used in this study were the same ones reported in the previous studies.[101,102] The lung, liver and skin samples were collected from 8 young (4-6 years old, 4 female and 4 male) and 8 old (18-21 years old, 4 female and 4 male) cynomolgus monkeys without clinical or experimental history. The HGPS cynomolgus monkeys were described in a previous study.[62] Primary hMPCs were isolated from the gingiva of individuals of the indicated age under the

approval from the Ethics Committee of the 306 Hospital of PLA in Beijing.[67] Human eyelid skin samples were obtained from blepharoplasty of the indicated healthy donors under ethical approval of Peking Union Medical College Hospital Institutional Review Board.[63] Human serum samples were collected under the approval of the Research Ethics Committee of the First Hospital of Kunming Medical University.[88] All human samples were obtained from healthy young and old donors. The age information of the human donors is listed in Table S2.

Cell culture

HEK293T cells and human fibroblasts were cultured in Dulbecco's Modified Eagle Medium (DMEM, Thermo Fisher Scientific) supplemented with 10% fetal bovine serum (FBS, GIBCO, Thermo Fisher Scientific), 2 mM GlutaMAX (Thermo Fisher Scientific), 0.1 mM non-essential amino acids (NEAA, Thermo Fisher Scientific), 1% penicillin/streptomycin (Thermo Fisher Scientific). Human MPCs (hMPCs) were grown on 0.1% gelatin (Sigma Aldrich)-coated plates (CORNING) in hMPC culture medium containing 90% MEMα (Thermo Fisher Scientific), 10% FBS, 2 mM GlutaMAX, 0.1 mM NEAA, 1% penicillin/streptomycin and 1 ng/mL bFGF (Joint Protein Central). Cells were cultured in an incubator (Thermo Fisher Scientific) at 37°C with 5% CO_2. WT hMPCs are replicatively senescent in their late passage (LP, P > 12), and prematurely senescent HGPS (*LMNA*$^{G608G/+}$) and WS (*WRN*$^{-/-}$) hMPC models exhibit growth arrest at passage 8-9 (referred to as LP in the premature aging model). HGPS and WS models were constructed via genome-editing in human embryonic stem cells (hESCs), followed by directed differentiation to hMPCs.[33] Human fibroblasts are replicatively senescent in their late passage (LP, P > 23).

METHOD DETAILS

Animal experiments

To evaluate whether lentiviral knockdown of MMTV alleviates aging-associated articular degeneration in mice, lentiviruses containing CRISPR-dCas9-KRAB-expressing empty backbone (CRISPRi-Control) or lentiviruses containing CRISPR-dCas9-KRAB and MMTV single-guide (sg) RNA (CRISRRi-sgMMTV) were injected into the articular cavities of 21-month-old mice twice with an interval of 4 weeks (n = 12 mice for each group). Grip strength was measured at 8 weeks after the first injection. To examine the effects of Abacavir on aging-associated articular degeneration, Abacavir was dissolved in PBS containing 1% DMSO at a final concentration of 5 mg/mL, and injected into the articular cavities of 22-month-old mice (n = 12 mice for each group) with a volume of 10 μL. Grip strength was measured at 8 weeks after the first injection. For long-term oral administration experiments, 18-month-old mice were treated daily with Abacavir dissolved in drinking water containing 0.4% DMSO at a final concentration of 1 mg/mL for a total of 3 mL, with 0.4% DMSO in drinking water as control (n = 23 mice for each group). The body weight, back, fur, skin, cataract and physical scoring, as well as the grip strength of mice were evaluated at 6, 12 and 24 weeks after treatment with Abacavir. The Y maze test was performed at 24 weeks after Abacavir treatment.

Grip strength test

The grip strength of the mice was assessed using a Grip Strength Meter (Panlab Grid Strength Meter, LE902). Briefly, four limbs of the mouse were placed on the top of the Grip Strength Meter and pulled along the direction of the grid at a constant rate until the Grip Strength Meter was released by the mouse. This process was repeated 10 times and the peak pull force at each time was recorded on a digital force transducer. The mean values from 10 consecutive trials were taken as the grip strength of each mouse. The number of mice (n) in each group is indicated in the figures; for example, n = 23 mice for vehicle or Abacavir in the drinking water as shown in Figure 7N; n = 12 mice injected with lentiviruses expressing control or sgMMTV using a CRISPRi system into the articular cavities as shown in Figure S7I; and n = 12 mice injected with vehicle or Abacavir into the articular cavities as shown in Figure S7L.

Y maze test

The Y maze test was performed using a Y-shaped arena consisting of three arms in identical lengths with 120° angles between each arm, a camera and a computer with tracking software. Briefly, the mouse was placed at the end of any arm of the Y maze, and allowed to explore the maze freely for 5 min. The camera system recorded the animal behavioural changes for 5 min. The total number of arm entries and the number of turns (alternating) reflecting that the mouse entered the three arms in a row were used to evaluate the short-term spatial memory. The number of mice (n) in each group is indicated in the figures; for example, n = 20 mice for vehicle and n = 22 for Abacavir in the drinking water as shown in Figure 7P.

In vivo bone histomorphometric analysis: Micro-Computed Tomography (Micro-CT)

The Micro-Computed Tomography (Micro-CT) scanning was conducted using a PE Quantum FX (PerkinElmer) on living mice. Briefly, the mice were anesthetized with isoflurane and scanned using the following settings. The proximal part of the tibias and the distal part of the femurs were scanned in a Micro-CT scanner with an isotropic voxel size of 18 μm. The X-ray tube voltage was set at 90 kV and the current was set at 160 μA, with an exposure time of 1 s. Quantification of the bone density was performed on the knee joint region of each mouse using Analyze 10.0 software. The number of mice (n) in each group is indicated in the figures; for example, n = 12 mice injected with lentiviruses expressing control or sgMMTV using a CRISPRi system into the articular cavities as shown in Figure 7G; and n = 10 mice injected with vehicle or n = 8 mice injected with Abacavir into the articular cavities as shown in Figure 7L.

Please cite this article in press as: Liu et al., Resurrection of endogenous retroviruses during aging reinforces senescence, Cell (2023), https://doi.org/10.1016/j.cell.2022.12.017

Western blotting

Cells were lysed in 1 × SDS buffer (100 mM Tris-HCl (pH = 6.8), 10% glycerol, 2% SDS and 2% 2-mercaptoethanol) and boiled at 105°C for 10 min. Protein concentration was measured with the BCA Kit (Dingguochangsheng Biotech). Cell lysates were subjected to SDS-PAGE electrophoresis and electrotransferred onto PVDF membranes (Millipore). Subsequently, the membranes were incubated with primary antibodies and then HRP-conjugated secondary antibodies. For chemiluminescent detection, western blots were incubated with substrates (substrate A: 0.2 mM coumaric acid, 1.25 mM luminal, 0.1 M Tris-HCl (pH = 8.5); substrate B: 3% H_2O_2), in a ratio of 1,000 μL of substrate A to 3 μL substrate B, or SuperSignal™ West Femto Maximum Sensitivity Substrate (Thermo Fisher Scientific). Imaging was performed with the Image Lab software on a ChemiDoc XRS+ system (Bio-Rad Laboratories, Inc.). Quantification of protein band intensity was performed using ImageJ. GAPDH was used as a loading control. Three independent experiments were performed (n = 3) for each assay. The number of animal (n) in each group is indicated in the figures; for example, n = 8 young and aged cynomolgus monkeys as shown in Figure 6B; n = 5 young and aged mice as shown in Figure S7B. The antibodies used for western blotting are listed in the key resources table.

Immunoprecipitation (IP) of HERVK from conditioned medium

Cells were cultured in hMPC medium supplemented with 10% microvesicle-depleted fetal bovine serum (dFBS) for 48 h, which was prepared via ultracentrifugation at 100,000 × *g* for 16 h.[103] Approximately 40 mL of conditioned medium from senescent cells was collected and filtered through a 0.2-μm filter (Pall Corporation) and pre-cleaned with Protein A/G Plus-Agarose (Santa Cruz Biotechnology) at 4°C for 2-3 h. Then, the harvested supernatants were incubated with a 1/1,000 dilution of HERVK-Env antibody (Austral Biologicals) and fresh Protein A/G Plus-Agarose at 4°C overnight. Finally, the supernatants were collected, and the beads were washed with PBS and subjected to western blotting.

Purification of microvesicle particles from conditioned medium

Cells were cultured in hMPC medium supplemented with 10% dFBS for 48 h before medium collection.[103] The conditioned medium was collected and the corresponding cell number was counted. Medium from the same number of cells was used for microvesicle purification by centrifugation at 300 × *g* for 10 min to eliminate cell contamination and 15,000 × *g* for 20 min, followed by filtration through a 0.2-μm filter (Pall Corporation) and then ultracentrifugation at 110,000 × *g* for 2 h.[103] Pellets were collected and resolved in an equal volume of PBS and subjected to viral RNA isolation or western blotting.

DNA/RNA isolation and quantitative (reverse transcription) PCR (qRT-PCR)

Total DNA from cells was extracted using the DNeasy Blood & Tissue Kit (Tiangen) following the manufacturer's instructions and then processed for qPCR analysis. Total cellular RNA was extracted using TRIzol (Thermo Fisher Scientific), subjected to DNase I treatment to remove genomic DNA contamination, and reverse transcribed to cDNA using the GoScript Reverse Transcription System (Promega). (RT-)PCR was performed using the THUNDERBIRD qPCR Mix (TOYOBO) on a CFX384 Real-Time System (Bio-Rad Laboratories, Inc.). 5S rDNA was used as an internal control for qPCR analysis of DNA, and *ACTB* or *GAPDH* was used as an internal control for qRT-PCR analysis of RNA. The number of animals or donors (n) in each group is indicated in the figures; for example, n = 4 human donors of young or old primary hMPCs as shown in Figure 2I; n = 8 young or aged cynomolgus monkeys as shown in Figures S6A, S6C, and S6D; n = 11 mice injected with lentiviruses expressing control or n = 12 mice injected with lentiviruses expressing sgMMTV using a CRISPRi system into the articular cavities as shown in Figure S7H; and n = 10 mice injected with vehicle, or n = 8 mice injected with Abacavir into the articular cavities as shown in Figure S7K. All primers used for qRT-PCR are listed in Table S5.

Viral RNA isolation from microvesicles

RNA was extracted from 140 μL of microvesicle suspension from the same number of cells using the QIAamp Viral RNA Mini Kit (-QIAGEN) following the manufacturer's instructions. Briefly, samples were incubated with pre-prepared buffer AVL and carrier RNA. After adding ethanol, the samples were loaded onto QIAamp Mini columns. After washing and elution, the eluted samples were treated with DNase I using a TURBO DNA-free Kit (Thermo Fisher Scientific). In brief, 2 μL DNase I and 2.4 μL reaction buffer were added to 20 μL eluted sample (viral RNA), followed by incubation at 37°C for 30 min. Subsequently, the DNase I was inactivated using the inactivation reagent and removed by centrifugation at 10,000 × *g* for 1.5 min. The collected supernatant was heated at 70°C for 10 min to inactive residual DNase I.

Droplet Digital PCR (ddPCR)

The purified viral RNA from microvesicles was reverse transcribed to cDNA using the GoScript Reverse Transcription System following the manufacturer's instructions. Then, 20 μL of reaction solution containing cDNA templates, primers and QX200 ddPCR EvaGreen Supermix (Bio-Rad Laboratories, Inc.) were mixed with 70 μL QX200™ Droplet Generation Oil for EvaGreen (Bio-Rad Laboratories, Inc.) in a DG8 cartridge (Bio-Rad Laboratories, Inc.) using a QX200 droplet generator (Bio-Rad Laboratories, Inc.). The droplet was transferred to a 96-well plate and sealed with a PX1™ PCR Plate Sealer (Bio-Rad Laboratories, Inc.). After PCR amplification with a thermal cycler (Bio-Rad Laboratories, Inc.), the samples were subsequently subjected to a QX200 droplet reader

Please cite this article in press as: Liu et al., Resurrection of endogenous retroviruses during aging reinforces senescence, Cell (2023), https://doi.org/10.1016/j.cell.2022.12.017

(Bio-Rad Laboratories, Inc.) to analyze the absolute copy number of HERVK in microvesicles from the same number of cells in each group. ddH_2O and cDNA from senescent hMPCs were used as negative and positive controls, respectively. Three biological replicates were performed for each group (n = 3).

ELISA

For the human IL6 ELISA assay, the medium was collected and filtered with a 0.2-μm filter and incubated in an anti-IL6 antibody-coated plate (BioLegend) according to the manufacturer's instructions. After incubation with a detection antibody, Avidin-HRP, freshly mixed TMB substrate, and stop solution, the plate was measured at 450 nm using a Synergy H1 Microplate Reader (BioTek). IL6 levels were normalized to the corresponding cell numbers. Three biological replicates were performed for each group (n = 3).

For HERVK-Env ELISA assay, conditioned medium or human serum was first concentrated into 100 or 10 times using Centricon Plus-70 (Millipore) or Amicon Ultra-15 (Millipore), respectively. The HERVK-Env protein in the conditioned medium or human serum was detected using the Human HERVK-Env Polyprotein ELISA Kit (CUSABIO) following the manufacturer's instructions. Briefly, 100 μL concentrated medium or serum was added into the coated plate and incubated for 2 h at 37°C. After incubation with Biotin-antibody, Avidin-HRP, freshly mixed TMB substrate and stop solution, the plate was measured at 450 nm using a Synergy H1 Microplate Reader. HERVK-Env levels in the conditioned medium were normalized to the corresponding cell numbers. Three biological replicates were performed for each group (n = 3). HERVK-Env levels in human serum were also quantified, with n = 30 donors in each group.

A 2'3'-cGAMP ELISA Kit (Cayman) was used to measure the levels of 2'3'-cGAMP in cells. Briefly, 50 μL of cell lysates from the same number of indicated cell lines were loaded onto the plate followed by incubation with 2'3'-cGAMP HRP tracer and 2'3'-cGAMP polyclonal antiserum for 2 h at room temperature with shaking. After incubation with TMB substrate and stop solution, the plate was measured at 450 nm using a Synergy H1 Microplate Reader. 2'3'-cGAMP levels were normalized to the corresponding cell numbers. Three biological replicates were performed for each group (n = 3).

Immunofluorescence, immunohistochemistry staining and microscopy

For immunofluorescence staining, cells seeded on coverslips (Thermo Fisher Scientific) were washed twice with PBS, fixed in 4% paraformaldehyde (PFA), permeabilized in 0.4% Triton X-100 in PBS and blocked with 10% donkey serum. Coverslips were incubated with primary antibodies in blocking buffer at 4°C overnight and then with secondary antibodies for 1 h at room temperature. Nuclei were labeled with Hoechst 33342 (Thermo Fisher Scientific). The co-staining of HERVK-Env and β-galactosidase was conducted using the Cellular Senescence Detection Kit-SPiDER-βGal (DOJINDO Laboratories). Briefly, cells seeded on coverslips were washed twice with PBS, fixed in 4% PFA for 3 min, and incubated with SPiDER-βGal for 30 min at 37°C. Then, the cells were washed with PBS and subjected to immunofluorescence staining of HERVK-Env following the normal procedure. Images were taken with a Leica SP5 confocal microscope or ZEISS confocal LSM900. The Z-stack 3D reconstruction of images was performed using IMARIS. For quantification of Ki67-positive cells, three biological replicates were set for each group (n = 3). Over 100 cells were quantified in each replicate. The quantification of HERVK-Env fluorescence intensity in each group was performed from more than 100 cells from 3 biological replicates.

Immunohistochemistry staining of tissue sections was performed using the DAB Staining Kit (ZSGB-BIO) according to the manufacturer's instructions. Briefly, deparaffinized sections using Xylene and ethanol, were incubated with 3% H_2O_2 solution to block endogenous peroxidase activity before antigen retrieval using 10 mM sodium citrate buffer (pH = 6.0). Sections were then permeabilized, blocked and incubated with primary antibodies at 4°C overnight and secondary antibodies for 1 h, followed by staining with DAB substrate solution and Hematoxylin, dehydration and mounting. To remove the background, the sections were washed with PBS 5 times for 5 min each time. Images were taken with a LEICA Aperio CS2 LSM900. The white balance was adjusted before capturing the images. The ratios of positive cells were quantified. The number of animals or donors (n) in each group is indicated in the figures; for example, n = 5, 7 or 8 young or aged cynomolgus monkeys as shown in Figure 6C; n = 5, 10, or 20 fields from two sections of WT and HGPS cynomolgus monkeys as shown in Figure 6F; n = 5 or 6 young or aged human donors of skin as shown in Figure 6H; n = 8 young or aged mice as shown in Figure 7A; n = 5, 6 or 8 young or aged mice as shown in Figure S7C; n = 7 or 10 young or aged mice as shown in Figure S7D; n = 8 or 11 young or aged mice as shown in Figure S7E; n = 12 mice injected with lentiviruses expressing control or sgMMTV using a CRISPRi system into the articular cavities as shown in Figure 7C; n = 10 or 11 mice injected with lentiviruses expressing control or sgMMTV using a CRISPRi system into the articular cavities as shown in Figure 7D; n = 11 mice injected with lentiviruses expressing control or sgMMTV using a CRISPRi system into the articular cavities as shown in Figure 7E; n = 11 or 12 mice injected with lentiviruses expressing control or sgMMTV using a CRISPRi system into the articular cavities as shown in Figure S7G; n = 8 or 9 mice injected with vehicle or Abacavir into the articular cavities as shown in Figure 7I; n = 7 or 8 mice injected with vehicle or Abacavir into the articular cavities as shown in Figure 7J; and n = 8 or 10 mice injected with vehicle or Abacavir into the articular cavities as shown in Figure S7J.

Safranin-O/Fast Green staining was performed by Servicebio Technology Co., Ltd. (Beijing, China). Briefly, sections were baked at 60°C overnight and cooled at room temperature for 20-30 min followed by deparaffinization and hydration in 70% ethanol. Then, the slides were stained with Weigert's Iron Hematoxylin for 7 min, 0.08% Fast Green for 3 min, and rinsed in 1.0% acetic acid for 10 s. After staining with 0.1% Safranin-O for 5 min and rinsing in 0.5% acetic acid and distilled water, sections were mounted. Images were

taken with a LEICA Aperio CS2 LSM900. The mean values from at least 6 regions of articular cartilages were taken as the thickness of articular cartilages of each mouse. The number of mice in each group is indicated in the figures; for example, n = 8 young or n = 11 aged mice as shown in Figure S7E; n = 12 mice injected with lentiviruses expressing control or sgMMTV using a CRISPRi system into the articular cavities as shown in Figure 7F; and n = 10 mice injected with vehicle or n = 8 mice injected with Abacavir into the articular cavities as shown in Figure 7K.

Antibodies used for immunofluorescence and immunohistochemistry staining are listed in the key resources table.

(sm)RNA/DNA-FISH

RNA-FISH was performed using the QuantiGene® ViewRNA ISH Cell Assay Kit (Thermo Fisher Scientific) following the manufacturer's instructions. Briefly, cells seeded on coverslips (Thermo Fisher Scientific) were fixed in fresh 4% formaldehyde solution, permeabilized with Detergent Solution QC and digested with Protease QC. Probe HERVK Alexa Fluor 488 was diluted in Probe Set Diluent QF and added to wells for 3 h at 41 + 1°C in an HB-1000 Hybridizer (Gene Company Limited). Coverslips were incubated with Working Pre-Amplifier Mix Solution for 30 min, Working Amplifier Mix Solution for 30 min and Working Label Probe Mix Solution for 30 min at 40 + 1°C in an HB-1000 Hybridizer, followed by PBS washing in each step. Nuclei were labeled with DAPI and slides were mounted and subjected to imaging with a Leica SP5 confocal microscope. HERVK RNA-FISH fluorescence intensity was quantified from more than 150 cells from 3 biological replicates.

Detection of HERVK mRNA and DNA in cytoplasm was performed via single-molecule (sm)-FISH. The targeting sequences of the probes for HERVK were split into pairs to increase the detection specificity, and probe pairs against HERVK were designed by Spatial FISH, Co., Ltd. Briefly, cells were fixed in 4% PFA in DEPC-treated PBS at room temperature for 20 min and washed for three times with DEPC-treated PBS, followed by 70% ethanol immersion for at least 24 h. Then, cells were treated with 0.2 M HCl in DEPC-treated H2O for 10 min and 5 μg/mL protein kinase K in DEPC-treated PBS for 5 min, respectively. For mRNA detection, cells were directly incubated with targeting probe pairs (10 μM for each probe) in hybridization buffer (10% deionized formamide, 2 × SSC, 10% dextran sulfate, and 2 mM VRC) at 42°C overnight. For detection of HERVK DNA, the cells were sequentially treated with RNase A (100 μg/mL in 2 × SSC) at 37°C for 1 h, 70% formamide in 2 × SSC at 72°C for 10 min, and a pre-cooled ethanol gradient (80%, 90%, 100%) for 1 min each gradient, followed by incubation with targeting probe pairs (10 μM for each probe) in hybridization buffer at 42°C overnight. After washing with washing buffer (2 × SSC, 30% formamide, 0.1% Triton-X 100, 2 mM VRC) three times, single-molecule detection of HERVK mRNA and DNA was realized using the following probes including amplification probes (SFSP-001 and SFTP-001 from Spatial FISH, Co., Ltd) and fluorescent probe (SFFP-001, Spatial FISH, Co., Ltd). Finally, the cells were counterstained with DAPI and imaged with a Leica SP5 confocal microscope or N-STORM. The relative number of fluorescent spots of HERVK DNA in the cytoplasm was quantified from over 10 cells in each sample. The targeting sequences of the probe pairs are listed in Table S5.

(Immuno-)Transmission electron microscopy (TEM)

Cells were pelleted and fixed with 2.5% (vol/vol) glutaraldehyde with Phosphate Buffer (PB) (0.1 M, pH = 7.4) at room temperature for 20 min and then at 4°C overnight. Routine heavy metal staining was conducted. Briefly, cells were postfixed with 1% (wt/vol) osmium tetraoxide in PB at 4°C for 2 h, dehydrated through a graded ethanol series into pure acetone, infiltrated in a graded mixture of acetone and resin, and then embedded in pure resin with 1.5% BDMA and polymerized at 45°C for 12 h, and then at 60°C for 48 h. Ultrathin sections (70-nm thick) were sectioned with a microtome (Leica EM UC6), and double-stained with uranyl acetate and lead citrate. For Immuno-TEM, cells seeded in 35-mm petri dishes (CORNING) were prefixed with 2% formaldehyde in warmed culture medium at 37°C in a cell incubator for 10 min, and with 4% formaldehyde at room temperature for 1 h and 4°C overnight, and then transferred into 1% formaldehyde. Samples were dehydrated through an ethanol gradient, infiltrated with a LR Gold resin gradient, and embedded in LR Gold resin containing initiator. Samples were then polymerized by UV light at -20°C for 24 h using a Leica AFS2 and sectioned using a Leica EM UC7. For staining, sections were blocked with 2% BSA in PB (Jackson ImmunoResearch), incubated with anti-HERVK-Env antibody at room temperature for 2 h, washed with PB buffer containing 0.1% cold fresh gelatin for 2 min for five times, incubated with 6-nm gold-labeled anti-mouse secondary antibody (Jackson ImmunoResearch) at room temperature for 1 h, and then fixed with 1% glutaraldehyde in ddH_2O. After washing with ddH_2O, sections were stained with 2% uranyl acetate at room temperature for 30 min and then processed for imaging using a TEM Spirit 120 kV (FEI Tecnai Spirit 120 kV). The number of RVLPs or HERVK RVLPs labeled with gold particles per cell was quantified from more than 40 cells in each group.

Plasmid construction

To generate HERVK[44,45] or STING knockdown vectors,[8] specific shRNAs were cloned into MluI/ClaI sites of the lentiviral vector pLVTHM (Addgene, #12247). To activate endogenous HERVK, non-targeting control sgRNA (sgNTC)[104] or sgRNA targeting HERVK LTR (sgHERVK)[42] was cloned into lentiSAM v2 vector (Addgene, #75112) via the ESP3I site, and then co-transfected into hMPCs with lentiMPH v2 (Addgene, #89308). The constructs that repress endogenous HERVK using a dCas9-KRAB-based system (CRISPRi-sgHERVK) and dCas9-KRAB-expressing empty backbone (CRISPRi-control) were kind gifts from the Dr. Didier Trono's lab (Ecole Polytechnique Fédérale de Lausanne (EPFL), Lausanne, Switzerland).[43] We investigated the target specificity of sgRNAs used for HERVK CRISPRa and CRISPRi systems. We first obtained the genomic locations of RepeatMasker-annotated repetitive elements

Please cite this article in press as: Liu et al., Resurrection of endogenous retroviruses during aging reinforces senescence, Cell (2023), https://doi.org/10.1016/j.cell.2022.12.017

based on the hg19 assembly, and then constructed the repetitive element BLAST (Basic Local Alignment Search Tool) database for *LTR5_Hs* (the promoter of HERVK). By comparing the sgRNA sequence with the constructed *LTR5_Hs* database, we found that ~30% of total *LTR5_Hs* elements showed good matches (expected value [E-value] < 1×10^{-5}) and were potentially targeted by CRISPRa and CRISPRi sgRNAs, which is highly consistent with the targeting efficiency of sgRNAs designed for HERVK transcriptional activation and/or repression in recently published studies.[105,106] To repress endogenous MMTV, the sgRNAs targeting the LTR region of MMTV (GenBank: AB049193.1) were designed by http://chopchop.cbu.uib.no/, and cloned into a dCas9-KRAB-expressing empty backbone via the BsmB1 site (CRISPRi-sgMMTV). To investigate the specificity of the sgRNA for MMTV, we first obtained the genomic locations for endogenous MMTVs annotated by RepeatMasker based on the mouse assembly (mm10 version) and found three potentially full-length MMTVs. By comparing the sgRNA sequence with the mouse LTR/ERVK elements, we found that the designed CRISPRi sgRNA showed high potential to target two of three potential full-length MMTVs (E-value < 0.05). The targeting sequences of shRNA or sgRNA are listed in Table S5.

To construct a plasmid producing HERVK RVLPs, full-length HERVK was synthesized according to a previously published sequence with NheI and ApaI sites at the N- and C-termini, respectively.[57,107] The KpnI site of pEGFP-N3 was disrupted using a Fast Mutagenesis System (TransGen), termed pEGFP-N3-KpnI'. HERVK was cloned into pEGFP-N3-KpnI' via NheI/ApaI sites, and its expression was driven by the CMV promotor of the vector. Of note, due to the stop signal in the 3'-LTR of HERVK, GFP in the vector backbone is not expressed in pricinple. Another CMV-EGFP cassette was PCR amplified from pEGFP-C1 and inserted into the KpnI site of pEGFP-N3-HERVK within the Env region of HERVK, which was designed following previously published studies.[58,108] To boost HERVK virus protein expression and improve RVLP production,[58,108] other HERVK expression plasmids including gag-pro-pol, env or rev fragments, were generated by PCR amplification using synthesized HERVK as the template, which was cloned into the pEGFP-N3 vector via NheI/ApaI sites for the Env fragment or KpnI/BamHI sites for the gag-pro-pol and rev fragments. Of note, to amplify the rev fragment, the reverse primer was designed to cover the additional 63 nucleotides at the C-terminal. In principle, the full-length HERVK containing LTR with the new CMV-EGFP cassette within the Env region could be packaged into RVLPs, but not other fragments.

Sequences of the sgRNAs used for CRISPRa and CRISPRi, as well as primers used for plasmid construction are listed in Table S5.

Production of HERVK RVLPs and lentiviruses

The production and purification of HERVK RVLPs were conducted by transfecting HEK293T cells with the full-length HERVK construct using Lipofectamine 3000 Transfection Reagent (Thermo Fisher Scientific). To boost the viral protein expression of HERVK and improve the production and transfection capacity of RVLPs, full-length HERVK with the CMV-EGFP cassette was co-transfected with other HERVK expression plasmids (encoding gag-pro-pol, env and rev) as well as VSG plasmid into HEK293T cells. The supernatants containing HERVK RVLPs were harvested at 48 h and 72 h after transfection, filtered with a 0.2-μm filter, and then concentrated by ultracentrifugation at 100,000 × *g* for 2 h. The vehicle was purified using the same procedure from the medium of HEK293T cells transfected with empty vector.

The lentivirus packaging was conducted according to previous studies.[70] HEK293T cells were transfected with lentiviral vectors together with the packaging plasmids pMD2.G (Addgene, #12260) and psPAX2 (Addgene, #12259) using Lipofectamine 3000 Transfection Reagent. Supernatants containing lentiviruses were harvested at 48 h and 72 h after transfection, filtered with a 0.2-μm filter, and concentrated by ultracentrifugation at 19,400 rpm for 2.5 h. The virus pellets were suspended and assessed for viral titers. The purification of viruses was performed under the safety rules of the Biological Safety Levels (BSL)-2 laboratory.

Cell treatment

5-AZA treatment was performed according to previous publications.[46,47] Briefly, WT hMPCs (P6) were seeded (recorded as passage 0 (P0) post-treatment) and treated with 500 ng/μL 5-AZA (dissolved in ddH_2O) for one passage (around 4-6 days). The medium supplemented with 5-AZA was changed every two days. Then, the cells were passaged and cultured in fresh medium. At P2 post-treatment (6 days after 5-AZA treatment), cells were harvested for Ki67 immunofluorescence staining, SA-β-gal activity analysis and RNA/DNA extraction.

The Abacavir treatment assay was conducted as described in a previous study.[53] Briefly, HGPS hMPCs (P7) were treated with different concentrations (0.2 μM, 1 μM and 10 μM) of Abacavir for two passages. During the treatment, cells were cultured with the culture medium being changed every two days, and the medium was supplemented with different concentrations (0.2 μM, 1 μM and 10 μM) of Abacavir. From the cell density and morphology, we found that treatment with the lowest concentration (0.2 μM) of Abacavir showed the best effect to alleviate premature senescence in HGPS hMPCs. Therefore, we used 0.2 μM as the final concentration for Abacavir treatment for the following experiments. After treatment, cells were collected for Ki67 immunofluorescence staining, SA-β-gal activity analysis and RNA/DNA extraction.

For infection with HERVK RVLPs, WT hMPCs (P6) were seeded (P0 post-treatment) and incubated with HERVK RVLPs in the presence of polybrene (Sigma-Aldrich) for 24 h. To increase the infection sensitivity of HERVK RVLPs, hMPCs were then subjected to centrifugation at 1,200 × *g* for 2.5 h. After culture for two passages, cells were processed for Ki67 immunofluorescence staining, SA-β-gal activity analysis and RNA/DNA extraction. To block the HERVK RVLPs, pretreatment with IgG or anti-HERVK-Env for 30 min in a 37°C incubator was performed.

For lentivirus transduction, WT hMPCs (P6), HGPS or WS hMPCs (P5) were seeded (P0 post treatment) and incubated with lentiviruses in the presence of polybrene for 24 h. After two passages, cells were processed for Ki67 immunofluorescence staining, SA-β-gal activity analysis and RNA/DNA extraction.

For conditioned medium treatment, 50% medium collected from the indicated cell culture with 50% fresh medium was mixed and used for culturing early-passage WT hMPCs (P5) in the presence of polybrene (Sigma-Aldrich) with the medium being changed every two days. The SC-CM (HGPS (P7), WS (P7) and WT (LP, P14)) also accelerated young hMPC senescence without polybrene, but it took a longer time to show effects. The cells were passaged and then collected for Ki67 immunofluorescence staining, SA-β-gal activity analysis and RNA/DNA extraction. To detect the RVLPs from conditioned medium adhering to the surface of young cells, cells were treated with conditioned medium for 12 h and subjected to TEM analysis.

To culture the cells with pooled human serum from young (18–25 years old, n = 5) or old individuals (65–80 years old, n = 5), primary hMPCs isolated from the gingiva of young donors were precultured in normal hMPC culture medium for 24 h. After washing with PBS three times, hMPCs were cultured in the medium containing 10% human serum for two passages and then collected for further analysis.

Clonal expansion assay

Five thousand cells were seeded in one well of a 6-well plate (Corning) precoated with gelatin (Sigma) and cultured for approximately 10 days. The cells were then fixed with 4% PFA for 30 min and stained with 10% crystal violet for 30 min. The relative cell integral density was calculated using ImageJ software. Three biological replicates are performed for each group (n = 3).

SA-β-gal staining

SA-β-gal staining was performed as described previously.[33,109] In brief, cells were fixed with a buffer containing 2% (w/v) formaldehyde and 0.2% (w/v) glutaraldehyde for 5 min and incubated with staining buffer containing 1 mg/mL X-gal at 37°C overnight. The optical microscope was used to observe SA-β-gal-stained cells and the percentage of SA-β-gal-positive cells was calculated using ImageJ software. Three biological replicates are performed for each group (n = 3). Over 100 cells were quantified in each replicate.

ChIP-qPCR

ChIP-qPCR was performed as previously described[110] with some minor modifications. Briefly, cells were fixed in 1% formaldehyde in PBS for 10 min at room temperature and then quenched by 125 mM glycine. Then, cells were lysed on ice for 10 min and subjected to sonication using a Covaris S220 Focused-ultrasonicator. The collected supernatants were incubated with Dynabeads Protein A (Thermo Fisher Scientific) pre-conjugated with 2.3 μg indicated antibodies or IgG at 4°C overnight. After washing, samples were digested with proteinase K (New England Biolabs) and reverse crosslinked at 68°C for 2 h on a thermomixer. DNA was extracted using phenol-chloroform-isoamyl alcohol and subjected to qPCR analysis. Three biological replicates were performed for each group (n = 3). Four technical replicates were performed for each biological replicate. For immunoprecipitation of cGAS, the cytoplasmic fraction of cells extracted after fixation[11] was incubated with anti-cGAS antibody- or IgG-conjugated Dynabeads Protein A at 4°C overnight. The DNA extraction procedure was performed as above. qPCR analysis of 5S rDNA, which was in principle absent in the cytoplasmic fraction, was used to exclude the nuclear genomic contamination. Four technical replicates were performed for each group (n = 4). The ChIP-qPCR data are presented as fold enrichment. Briefly, the negative control (IgG) sample is given a value of '1', and everything else will then be normalized as a fold change of this negative control sample. The primers used for ChIP-qPCR are listed in Table S5.

Strand-specific RNA sequencing (RNA-seq)

Strand-specific RNA-seq libraries were prepared and sequenced by Novogene Bioinformatics Technology Co. Ltd. In brief, total RNA was extracted from 1 × 10^6 cells per duplicate using TRIzol reagent, and genomic DNA was removed. RNA concentrations were measured using a Qubit™ RNA Assay Kit with a Qubit® 2.0 Fluorometer (Thermo Fisher Scientific). A total amount of 3 μg RNA per sample was used for the RNA sample preparations and library constructions. Then, ribosomal RNA was removed using the Epicentre Ribo-Zero™ rRNA Removal Kit (Epicentre), and rRNA-free residue was discarded by ethanol precipitation. Sequencing libraries were prepared using the NEBNext® Ultra™ Directional RNA Library Prep Kit for Illumina® (New England Biolabs) following the manufacturer's instructions. High-throughput sequencing was performed on an Illumina NovaSeq 6000 platform.

RNA-seq data processing

The processing pipeline for RNA-seq data has been reported previously.[71,101] Pair-end raw reads were trimmed by TrimGalore (version 0.4.5) (Babraham Bioinformatics) (https://github.com/FelixKrueger/TrimGalore) and mapped to the human (*Homo sapiens*) hg19 or cynomolgus macaque (*Macaca Fascicularis*) MacFas5.0 reference genome obtained from the UCSC genome browser database using STAR (version 2.7.1a) or hisat2 (version 2.0.4).[92,95] High-quality mapped reads (score of mapping quality more than 20) were then used for counting reads by HTSeq (version 0.11.0) or featureCounts (version 1.6.4).[93,94] Differentially expressed genes (DEGs) were calculated by the DESeq2 R package (version 1.29.8) with the cutoff "$|\log_2(\text{fold change})| > 0.5$ and adjusted p value < 0.05" for hMPCs.[97] SASP genes were obtained from a previous study.[9] Gene set enrichment analysis (GSEA) was conducted by GSEA application (version 2.2.4).[90]

Please cite this article in press as: Liu et al., Resurrection of endogenous retroviruses during aging reinforces senescence, Cell (2023), https://doi.org/10.1016/j.cell.2022.12.017

Analysis of the expression levels of repetitive elements

To evaluate the expression levels of repetitive elements, the cleaned reads were mapped to the human (*Homo sapiens*) hg19 reference genome using STAR software (version 2.7.9a) with the parameter "–outFilterType BySJout –winAnchorMultimapNmax 100 –outFilterMultimapNmax 100 –outFilterMismatchNoverLmax 0.04".[95] Transposable element quantification and the differential analysis were computed using the TEtranscripts software (version 2.2.1).[96] In brief, TEtranscripts simultaneously counted the gene abundances and transposon abundances and utilized R package DESeq2 (version 1.26.0) for the differential analysis. Then, differentially expressed repetitive elements were computed with a cutoff "$|\log_2(\text{fold change})| > 0.2$ and FDR < 0.05". Class for repetitive elements was annotated within RepeatMasker, which can be classified as LTR, LINE, SINE, DNA (also known as DNA transposons), satellite, and some RNA repeats.

Whole genome bisulfite sequencing (WGBS) library construction and sequencing

Library preparation and sequencing for WGBS were performed as previously reported.[111] In brief, genomic DNA was extracted from 2×10^6 cells per duplicate using DNeasy Blood & Tissue Kits (QIAGEN) and sheared to 100-300 bp with a sonicator. Then, bisulfite treatment, library preparation, quality control and sequencing were conducted by Novogene Bioinformatics Technology Co. Ltd.

WGBS data processing

WGBS data analysis was performed as previously reported.[111] In brief, raw sequencing reads were trimmed by fastp software (version 0.19.10) with default parameters.[91] Then, cleaned reads were mapped to the human (*Homo sapiens*) hg19 reference genome obtained from the UCSC genome browser database using bsmap (version 2.90) with parameters "-v 0.1 -g 1 -R -u".[98] CpG DNA methylation levels for each cytosine site were calculated by the methratio program provided by bsmap. To ensure the accuracy of methylation level detection, forward and reverse strand reads for each CpG site were combined and only CpG sites with a depth of more than 5 were kept for downstream analysis. To calculate the relative CpG DNA methylation level in repetitive element loci, we obtained the genomic loci for each RepeatMasker-annotated repetitive element from the UCSC genome browser. Then, the average CpG DNA methylation level for each RepeatMasker-annotated repetitive element was calculated, and the statistical analysis was conducted by the ggpubr R package (version 0.4.0) in R (version 4.0.2).

QUANTIFICATION AND STATISTICAL ANALYSIS

All data were statistically analyzed using the PRISM version 8 software (GraphPad Software). Results are presented as the mean ± SEM. Comparisons were conducted using the two-tailed student's t test or one-way ANOVA. p values < 0.05 were considered statistically significant (*), p values < 0.01 and p values < 0.001 were considered highly statistically significant (** and ***).

Supplemental figures

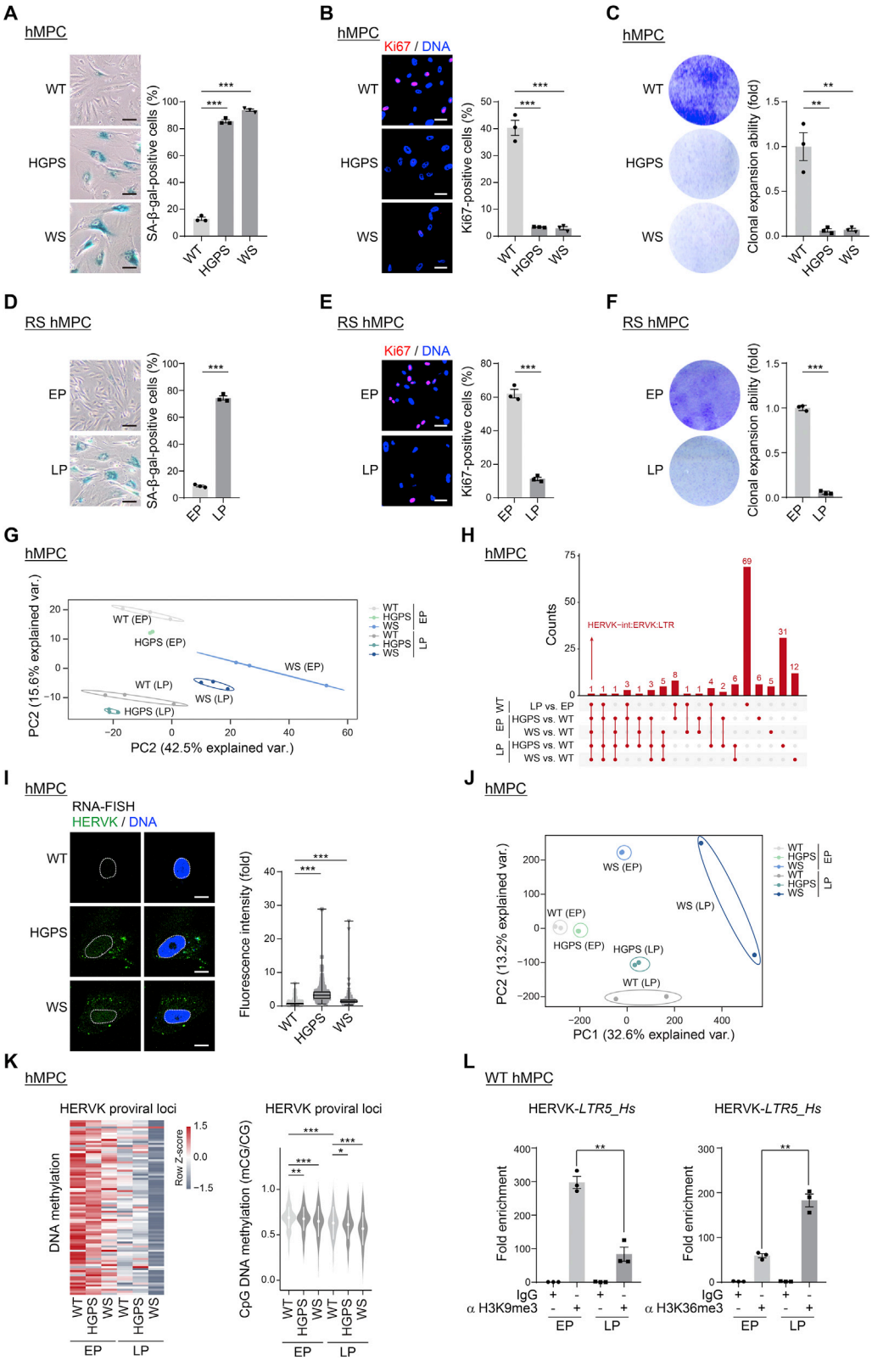

(legend on next page)

Figure S1. Increased expression of HERVK in senescent hMPCs, related to Figure 1

(A–F) SA-β-gal, Ki67 staining, and clonal expansion assay of WT, HGPS, and WS hMPCs, as well as WT hMPCs at EP and LP.

(G and H) Principal component analysis (PCA) of RNA-seq data based on the normalized read count of repetitive elements (G), and UpSet plot showing the overlap of upregulated RepeatMasker-annotated repetitive elements (H) in RS and prematurely senescent hMPCs.

(I) HERVK RNA-FISH analysis in WT, HGPS, and WS hMPCs.

(J and K) PCA of the whole-genome CpG DNA methylation levels (J) and CpG methylation levels at the HERVK proviral genomic locus (K) in RS and prematurely senescent hMPCs.

(L) ChIP-qPCR analysis of H3K9me3 and H3K36me3 enrichment in HERVK-*LTR5_Hs* regions in RS hMPCs.

Scale bars: 20 μm in (A), (B), (D), and (E); and 10 μm in (I).

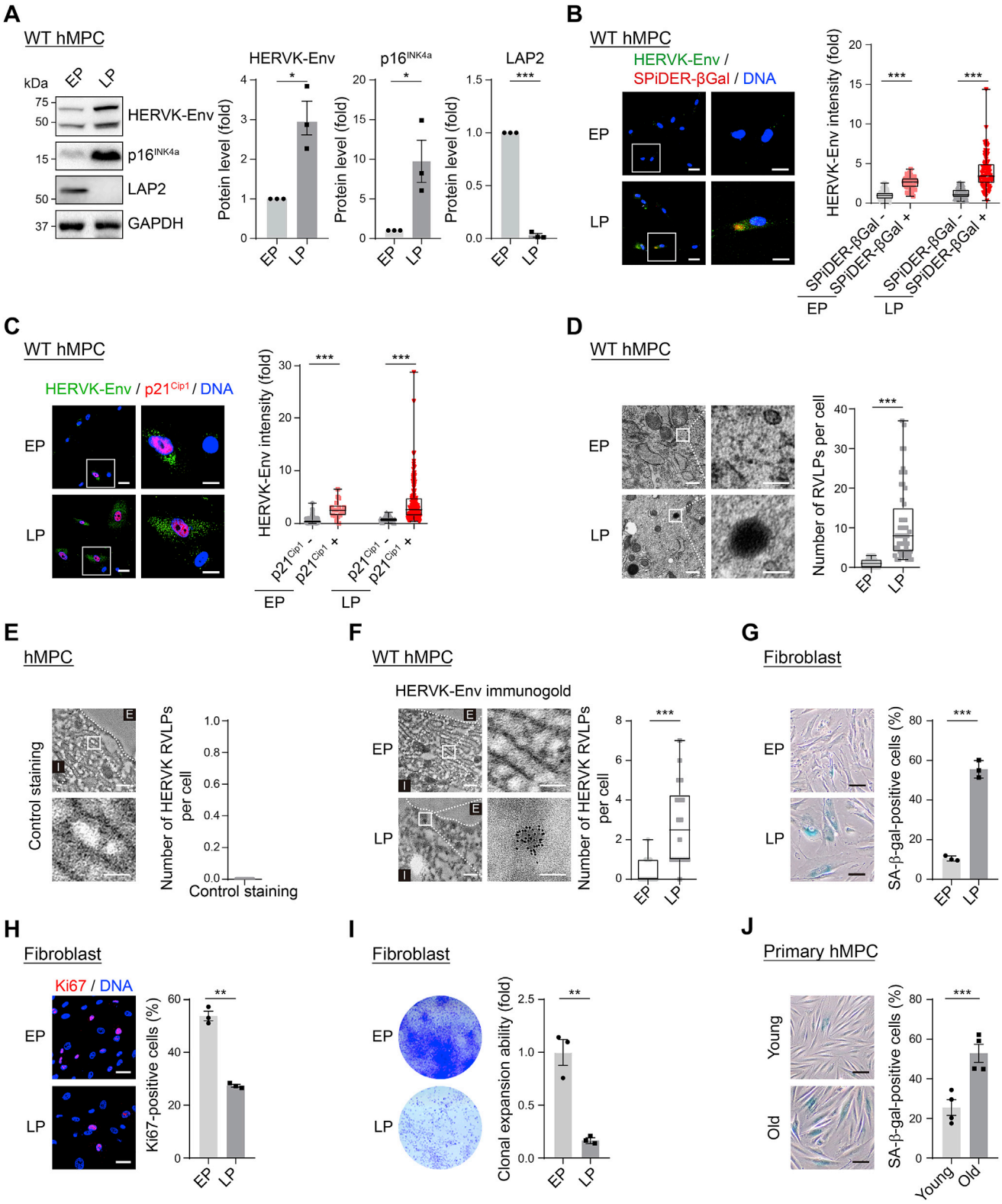

Figure S2. Increased HERVK proviral components in senescent cells, related to Figure 2

(A–C) Western blotting of HERVK-Env, p16^{INK4a}, and LAP2 (A), immunofluorescence co-staining of HERVK-Env and SPiDER-βGal (B) or p21^{Cip1} (C) in RS WT hMPCs.

(legend continued on next page)

(D–F) TEM analysis (D), and TEM analysis after negative immunogold labeling without the primary antibody (E), or immunogold labeling with anti-HERVK-Env antibody (F) in RS WT hMPCs.

(G–J) SA-β-gal, Ki67 staining, and clonal expansion assay of RS human fibroblasts (G–I), as well as SA-β-gal staining of primary hMPCs from young and old donors (J).

Scale bars: 20 and 10 μm (zoomed-in images) in (B) and (C); 200 and 100 nm (zoomed-in images) in (D)–(F); and 20 μm in (G), (H), and (J).

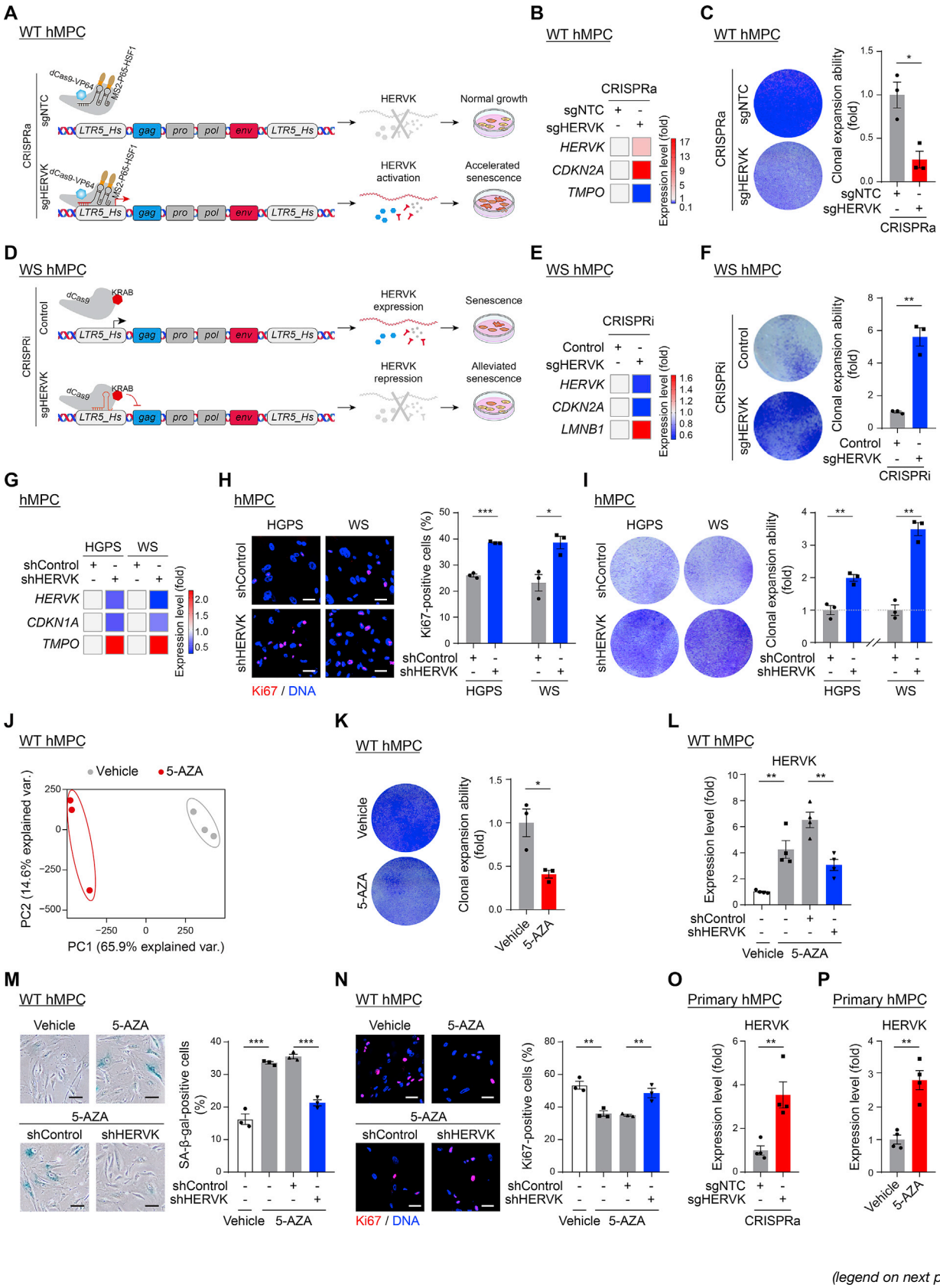

(legend on next page)

Figure S3. The upregulation of HERVK drives hMPC senescence, related to Figure 3

(A–F) Schematic diagram of the experimental procedure (A), heatmap showing the qRT-PCR analysis of HERVK and senescence marker genes (B), and clonal expansion assay (C) in WT hMPCs transduced with lentiviruses expressing sgNTC or sgHERVK using a CRISPRa system, or those in WS hMPCs transduced with lentiviruses expressing control or sgHERVK using a CRISPRi system (D–F).

(G–I) Heatmap showing the qRT-PCR analysis of HERVK and senescence marker genes (G), Ki67 staining (H), and clonal expansion assay (I) of HGPS or WS hMPCs after transduction with lentivirus delivering shControl or shHERVK.

(J and K) PCA of the whole-genome CpG DNA methylation levels (J) and clonal expansion assay (K) in vehicle- or 5-AZA-treated WT hMPCs.

(L–N) qRT-PCR analysis of the HERVK levels (L), SA-β-gal (M), and Ki67 staining (N) of vehicle- or 5-AZA-treated WT hMPCs after HERVK knockdown.

(O and P) qRT-PCR analysis of the HERVK levels in primary hMPCs from a young individual transduced with lentiviruses expressing sgNTC or sgHERVK using a CRISPRa system (O) or that treated with vehicle or 5-AZA (P). Scale bars, 20 μm (all panels).

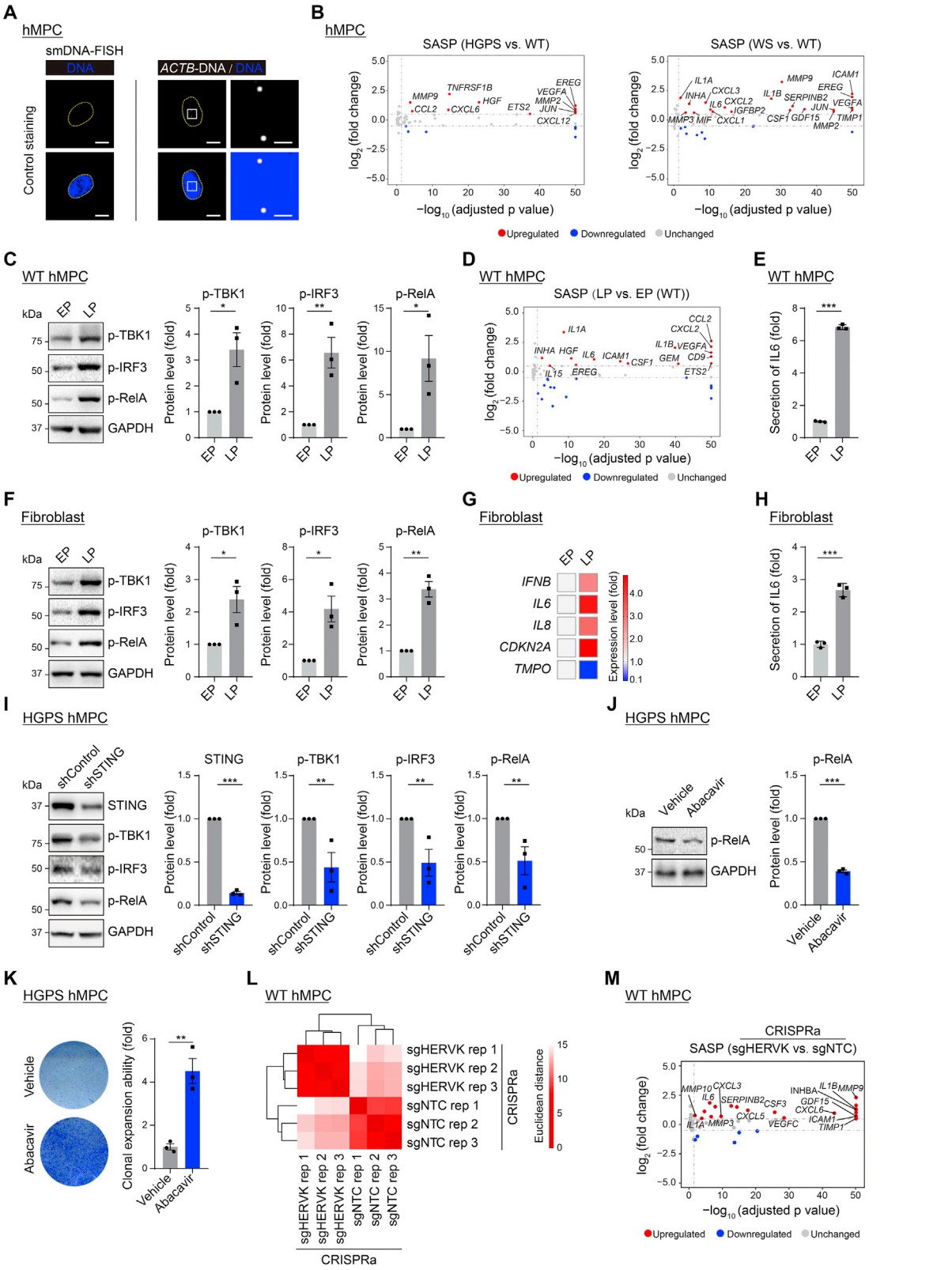

(legend on next page)

Figure S4. The innate immune response is activated in senescent cells, related to Figure 4

(A) Negative and positive control staining (*ACTB*) for smDNA-FISH in hMPCs.

(B) Scatter plots showing the differential expression levels of SASP genes in HGPS or WS hMPCs compared with WT hMPCs at LP.

(C–E) Western blotting of p-TBK1, p-IRF3, and p-RelA (C), as well as scatter plot showing the differential expression levels of SASP genes (D) and ELISA analysis of IL-6 levels in the culture medium (E), in RS WT hMPCs.

(F–H) Western blotting of p-TBK1, p-IRF3, and p-RelA (F), as well as qRT-PCR analysis of SASP genes (G) and ELISA analysis of IL6 levels in culture medium (H) in RS fibroblasts.

(I) Western blotting of STING, p-TBK1, p-IRF3, and p-RelA in HGPS hMPCs after STING knockdown.

(J and K) Western blotting of p-RelA (J) and clonal expansion assay (K) in HGPS hMPCs treated with Abacavir.

(L and M) Heatmap showing the Euclidean distance analysis to evaluate the reproducibility of the RNA-seq (L) and scatter plots showing the differential expression levels of SASP genes (M) in WT hMPCs transduced with the lentivirus expressing sgNTC or sgHERVK using the CRISPRa system. Scale bars, 10 μm and 200 nm (zoomed-in images) in (A).

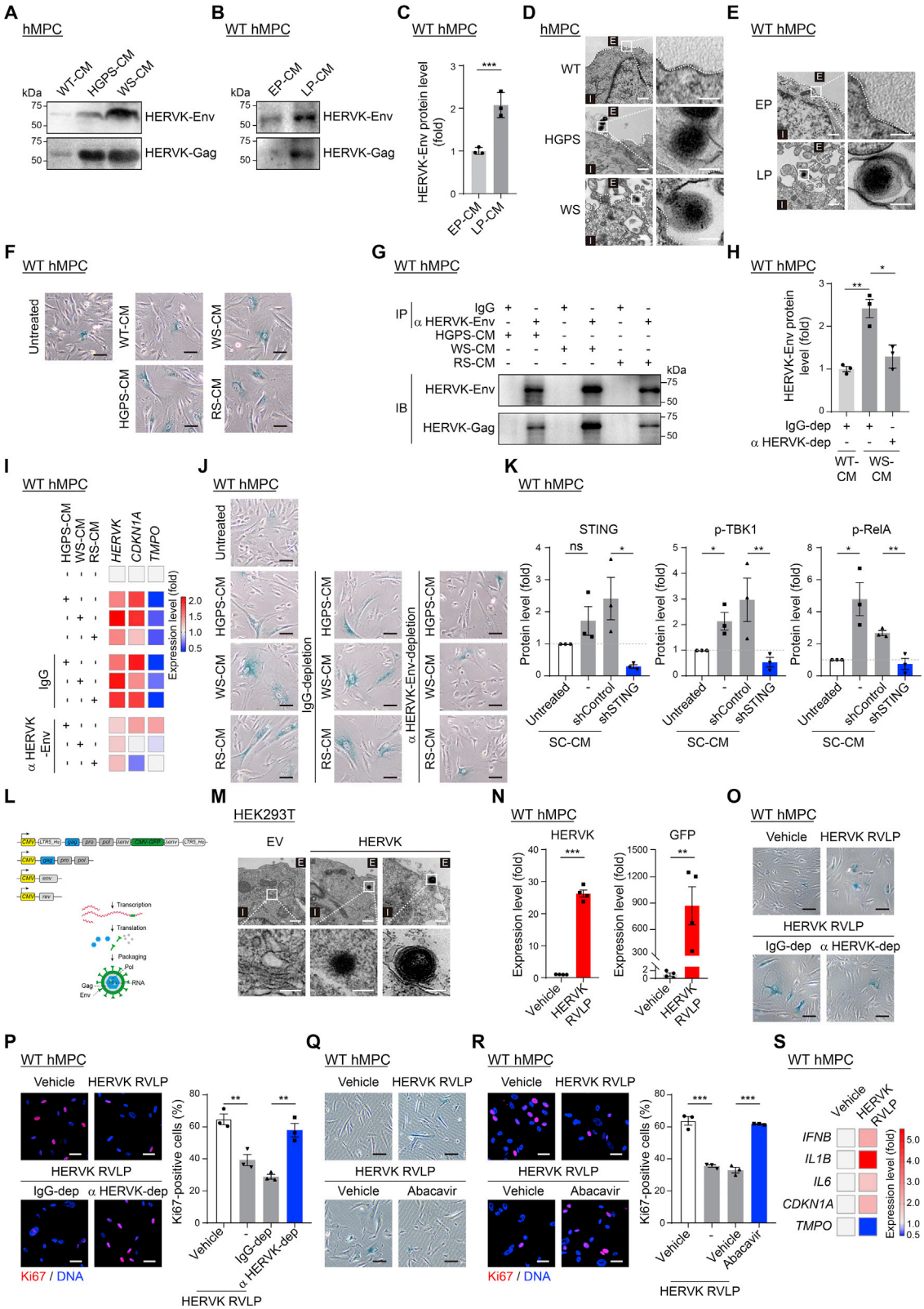

(legend on next page)

Figure S5. HERVK released from senescent cells induces young cell senescence, related to Figure 5

(A and B) Western blotting of HERVK-Env and -Gag in microvesicles from CM of WT, HGPS, and WS hMPCs (A), as well as RS WT hMPCs (B).

(C) ELISA analysis of relative HERVK-Env levels in the CM of RS WT hMPCs.

(D and E) TEM images of WT, HGPS, and WS hMPCs (D), as well as RS WT hMPCs (E).

(F) Representative images of SA-β-gal staining for Figure 5G.

(G–J) Western blotting of HERVK-Env and -Gag in the immunoprecipitates of SC-CM (G), ELISA analysis of relative HERVK-Env protein levels in the SC-CM (H), and heatmap showing qRT-PCR analysis of the HERVK levels (I) and representative images of SA-β-gal staining for Figure 5I (J) in WT hMPCs treated with SC-CM, after immunodepletion with IgG or anti-HERVK antibody.

(K) Statistical results for western blotting of STING, p-TBK1, and p-RelA in Figure 5J.

(L and M) Schematic diagram showing the constructs to produce HERVK RVLP (L), and TEM images of HEK293T cells transfected with empty vector (EV) or HERVK constructs (M).

(N and O) qRT-PCR analysis showing the levels of HERVK and GFP (N), and representative images of SA-β-gal staining for Figure 5O (O) in WT hMPCs infected with HERVK RVLPs.

(P) Immunofluorescence staining of Ki67 in WT hMPCs infected with HERVK RVLPs after pretreatment with IgG or anti-HERVK-Env antibody.

(Q and R) Representative images of SA-β-gal staining for Figure 5P (Q) and immunofluorescence staining of Ki67 (R) in WT hMPCs infected with HERVK RVLPs in the presence of Abacavir.

(S) Heatmap showing the qRT-PCR analysis of the expression levels of SASP genes and senescence marker genes in WT hMPCs treated with vehicle or HERVK RVLPs. Scale bars, 200 and 100 nm (zoomed-in images) in (D), (E), and (M); and 20 μm in (F), (J), and (O)–(R).

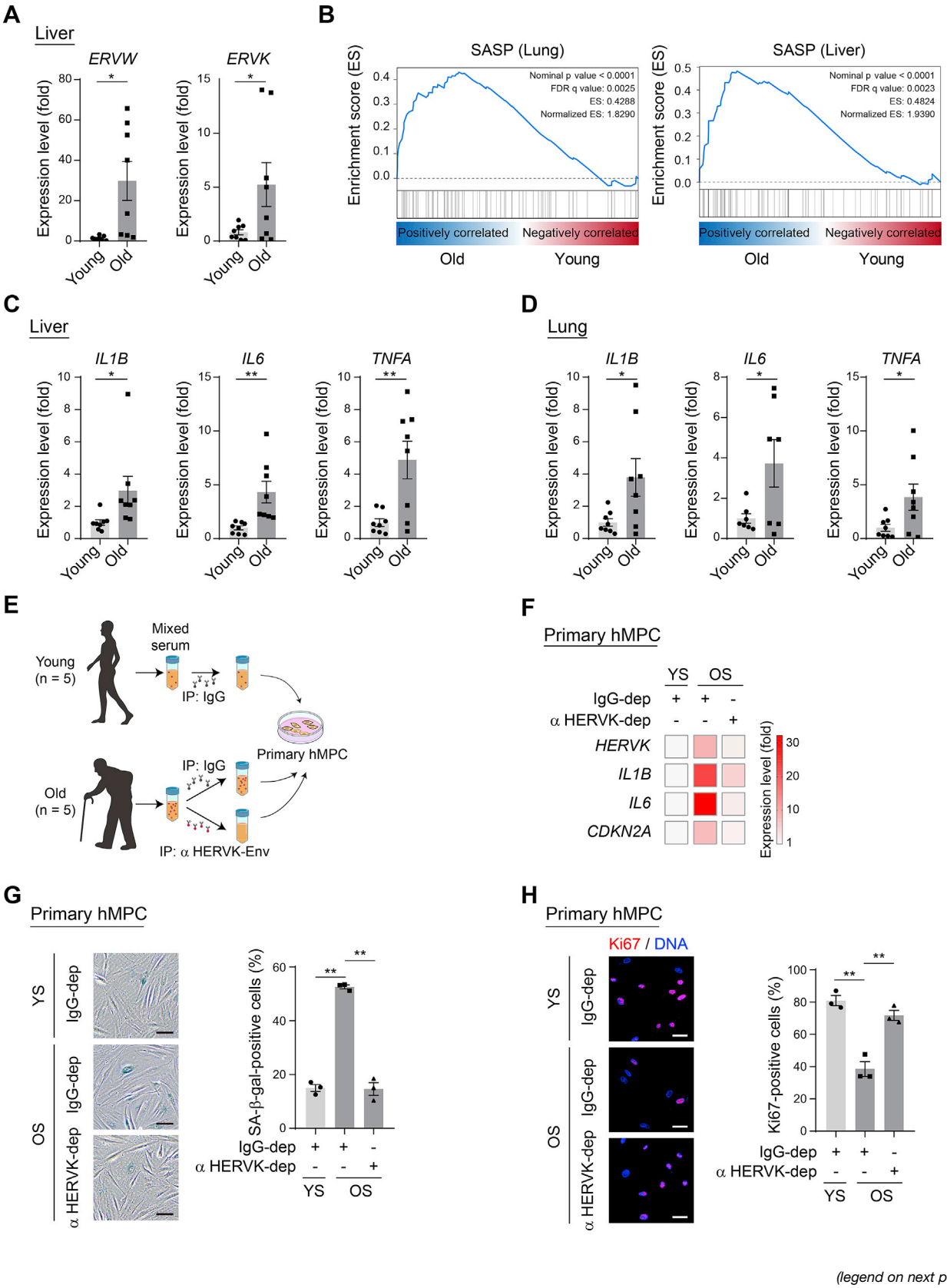

(legend on next page)

Figure S6. Activation of endogenous retrovirus and the innate immune pathway *in vivo*, related to Figure 6

(A–D) qRT-PCR analysis of the levels of ERVW and ERVK in the livers (A), gene set enrichment analysis (GSEA) of SASP gene levels in lungs and livers (B), and qRT-PCR analysis of the levels of SASP genes in the livers (C) and lungs (D) of young and old cynomolgus monkeys.

(E–H) Schematic diagram showing the experimental procedure (E), qRT-PCR analysis of the expression levels of HERVK, SASP genes, and senescence marker genes (F), as well as SA-β-gal (G) and Ki67 (H) staining of young primary hMPCs cultured with medium containing young (YS) or old sera (OS) after immunodepletion with IgG or anti-HERVK antibody. Scale bars, 20 μm (all panels).

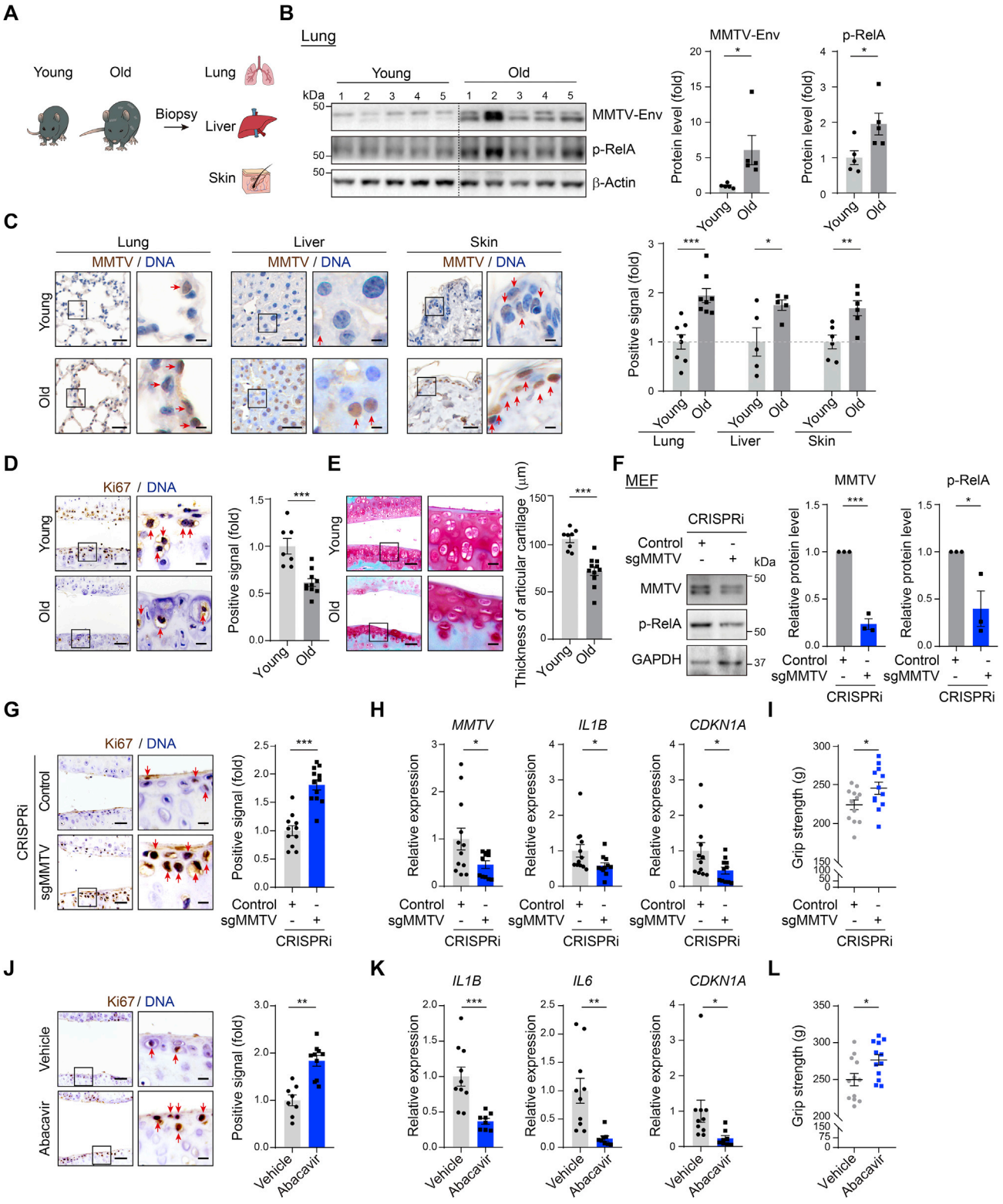

Figure S7. Suppression of endogenous retrovirus alleviates tissue aging in mice, related to Figure 7

(A–C) Schematic diagram of samples (A), western blotting of MMTV and p-RelA in the lungs (B), and immunohistochemistry analysis of MMTV in the lungs, livers, and skin (C), from young and old mice.

(D and E) Immunohistochemistry analysis of Ki67 (D) and Safranin-O/Fast Green (E) staining in the articular cartilages of young and old mice.

(legend continued on next page)

(F) Western blotting of MMTV and p-RelA in MEFs transduced with lentiviruses expressing control or sgMMTV using a CRISPRi system.
(G–I) Immunohistochemistry analysis of Ki67 (G), qRT-PCR analysis of the levels of *MMTV*, *IL1B*, and *CDKN1A* in the articular cartilages (H), and grip strength analysis (I) of mice intra-articularly injected with lentiviruses expressing control or sgMMTV using a CRISPRi system.
(J–L) Immunohistochemistry analysis of Ki67 (J), qRT-PCR analysis of the levels of *IL1B*, *IL6*, and *CDKN1A* levels in the articular cartilages (K), and grip strength analysis (L) of mice intra-articularly injected with vehicle or Abacavir. Scale bars, 50 and 10 μm (zoomed-in images) (all panels).